Meteoritics & Planetary Science 32, 395–412 (1997)

Experimental rare-earth-element partitioning in oldhamite: Implications for the igneous origin of aubritic oldhamite

TAMARA L. DICKINSON[1]* AND TIMOTHY J. McCOY[2,3]

[1]Physics Department, Catholic University of America, Washington, D.C. 20064, USA
[2]Code SN4, NASA Johnson Space Center, Houston, Texas 77058, USA
[3]Department of Mineral Sciences, MRC 119, National Museum of Natural History, Smithsonian Institution, Washington, D.C. 20560, USA
*Correspondence author's e-mail address: u1tld@lepvax.gsfc.nasa.gov

(Received 1996 February 28; accepted in revised form 1997 March 4)

Abstract–Aubritic oldhamite (CaS) has been the subject of intense study recently because it is the major rare-earth-element (REE) carrier in aubrites, has a variety of REE patterns comparable to those in unequilibrated enstatite chondrites and has an extraordinarily high melting point as a pure substance (2525 °C). These latter two facts have caused some authors to assert that much of the aubritic oldhamite is an unmelted nebular relict, rather than of igneous origin. We have conducted REE partitioning experiments between oldhamite and silicate melt using an aubritic bulk composition at 1200 °C and 1300 °C and subsolidus annealing experiments. All experiments produced crystalline oldhamite, with a range of compositions, glass and Fe metal, as well as enstatite, SiO_2, diopside and troilite in some charges. Rare-earth-element partitioning is strongly dependent on oldhamite composition and temperature. Subsolidus annealing results in larger partition coefficients for some oldhamite grains, particularly those in contact with troilite. All experimental oldhamite/silicate melt partition coefficients are <20 and the vast majority are <5, which is similar to those reported in the literature and is two orders of magnitude less than those inferred for natural aubritic oldhamite. These partition coefficients preclude a simple igneous model, since REE abundances in aubritic oldhamite are greater than would be predicted on the basis of the experimental partition coefficients. Our experimental partition coefficients are consistent with a relict nebular origin for aubritic oldhamite, although experimental evidence that suggests melting of oldhamite at temperatures lower than that reached on the aubrite parent body are clearly inconsistent with the nebular model. Our experiments are consistent also with a complex igneous history. Oldhamite REE patterns may reflect a complex process of partial melting, melt removal, fractional crystallization and subsolidus annealing and exsolution. These mechanisms (primarily fractional crystallization and subsolidus annealing) can produce a wide range of REE patterns in aubritic oldhamite, as well as elevated (100–1000 × CI) REE abundances observed in aubritic oldhamite.

INTRODUCTION

Aubrites (enstatite achondrites) are breccias consisting predominantly of FeO-free enstatite and a host of unusual phases formed under highly reducing conditions (Watters and Prinz, 1979). Among these minor phases are numerous sulfides in which normally lithophile elements (*e.g.*, Ca, Mg, Mn and Cr) behave as chalcophile elements. Aubrites are of interest because of their similarities in mineralogy (Keil, 1968; Watters and Prinz, 1979) and O-isotopic composition (Clayton *et al.*, 1984) to enstatite chondrites. These two groups of meteorites may provide our best opportunity to study related meteorites ranging from primitive chondrites to achondrites. Several authors have argued that aubrites are the products of direct condensation from the solar nebula (Wasson and Wai, 1970; Richter *et al.*, 1979; Sears, 1980). Based on textural evidence in Norton County (see Keil, 1989), some recent authors favor an igneous origin for the various aubrite lithologies that are now represented as clasts in breccias.

Many of these same arguments concerning the origin of aubrites have been renewed recently and focus not on aubrites as a whole but on a specific mineral within aubrites, oldhamite (CaS). As the major rare-earth-element (REE) carrier in aubrites (*e.g.*, Kurat *et al.*, 1992; Floss *et al.*, 1990; Lodders *et al.*, 1993; and Wheelock *et al.*, 1994), oldhamite has garnered special attention. In addition, oldhamite has two unique characteristics that have led to vigorous debate about its origin. It has an extraordinarily high melting temperature as a pure substance (2450–2525 °C; Vogel and Heumann, 1941; Chase *et al.*, 1985), and some oldhamite grains exhibit REE abundances and patterns that are similar to those of unequilibrated enstatite chondrites (UECs) (*e.g.*, Floss and Crozaz, 1993; Crozaz and Lundberg, 1995). Several authors have taken these facts to suggest that many oldhamite grains did not crystallize from the aubrite magma but rather are nebular relicts that survived igneous processing (*e.g.*, Kurat *et al.*, 1992; Floss and Crozaz, 1993; Lodders *et al.*, 1993; Lodders, 1995, 1996a,b). In contrast, textural evidence from an oldhamite-dominated clast in Norton County (Wheelock *et al.*, 1994) and REE patterns in some aubritic oldhamite (Floss and Crozaz, 1993) favor an igneous parentage. It is worth noting that some authors (*e.g.*, Floss and Crozaz, 1993) favor a mixed origin where some oldhamite grains are nebular relicts while others crystallized from the aubrite melt. Some authors have combined the apparent contradiction between REE patterns and igneous textures to suggest that oldhamite does have an igneous origin, but that origin was in an impact melt where equilibrium was not attained (*e.g.*, Lodders and Palme, 1989; Shimaoka *et al.*, 1995). In addition, Wheelock *et al.* (1994) inferred that oldhamite/silicate partition coefficients in natural systems should be on the order of 100–1000, based on ion microprobe data of naturally occurring oldhamite in Norton County and comparison with the bulk REE inventory of this aubrite. However, most experimentally determined partition coefficients reported to date are generally <5 (Dickinson *et al.*, 1990a,b,c, 1991; Lodders and Palme, 1989, 1990; Lodders *et al.*, 1990; Lodders, 1995, 1996a,b).

Thus, the debate about the origin of oldhamite has renewed interest in models for aubrite formation.

In spite of this renewed interest in the genesis of aubrites and the important role played by oldhamite, very little is known about the melting and crystallization behavior of oldhamite in complex assemblages or about the partitioning of REEs between oldhamite and silicate liquids under highly reducing conditions. Preliminary experiments by Jones and Boynton (1983) using a eucritic starting composition produced two immiscible sulfide-rich liquids (Ca-Mg-rich and Fe-rich). Silicate liquid/sulfide liquid partition coefficients ranged from ~0.5–2.0. Equilibration experiments between CaS and a melt similar to the silicate portion of enstatite chondrites (Lodders and Palme, 1989, 1990; Lodders *et al.*, 1990; Lodders, 1995, 1996a,b) resulted in oldhamite/silicate partition coefficients generally less than unity. We report here the results of our oldhamite/silicate liquid partitioning experiments using an aubritic-like starting composition. In addition, we have acquired data on the crystallization behavior of oldhamite in our experiments (*e.g.*, crystallization order and oldhamite crystallization temperature).

EXPERIMENTAL TECHNIQUES

In partitioning studies, it is important to produce phases compositionally similar to natural phases. Oxygen fugacities lower than achievable in traditional CO-CO_2 gas-mixing furnaces were needed to obtain the compositions of interest. In order to achieve these low O fugacities, some metallic phases, rather than oxides or sulfides, were used in the starting material to serve as O getters. An experiment was considered successful if: (a) plagioclase did not crystallize, (b) a low O fugacity was achieved (as indicated by low FeO contents in the glass, the presence of Si in metallic Fe and the presence of oldhamite) and (c) the oldhamite approached natural compositions (~50 mol% Ca).

Starting Materials and Run Conditions

Our initial starting composition (Dickinson *et al.*, 1990a) consisted of oxides of Si, Al, Ca, Mg and Fe that approximated a eucrite composition and powdered metallic Fe, Ni, and FeS_2 (Table 1). This composition and experimental technique was similar to that used in reconnaissance experiments by Jones and Boynton (1983). Aluminum foil or Al-powder was added to the starting material as an O getter. However, these initial experiments crystallized plagioclase due to the Al-enrichment. Dickinson *et al.* (1990b,c) used a significantly different starting composition (Table 1), which among other things was enriched in Ca and S to promote the crystallization of CaS. However, this starting composition produced sulfide that was less calcic than natural oldhamite (~50 mol% Ca). Because of the early plagioclase crystallization and the Ca-poor sulfide composition, these experiments (Dickinson *et al.*, 1990a,b,c) did not satisfactorily simulate aubrite crystallization. Thus, these results are not relevant to the question of the origin of aubritic oldhamite and, therefore, will not be discussed in detail in this paper.

The next generation of experiments (Dickinson *et al.*, 1991 and this work) used a different starting composition (Table 1) in order to suppress early plagioclase crystallization and to produce more calcic sulfides. This composition more closely approximated aubrites (Watters and Prinz, 1979) but was not identical to an actual aubrite composition because such a composition will not crystallize numerous oldhamites large enough to be analyzed using the electron microprobe. Our starting composition was depleted in Si and Mg and slightly enriched in Fe relative to aubrites. In addition, this starting composition was enriched in Al, which was used as an O getter, and significantly enriched (~10×) in Ca and S in order to produce abundant CaS grains large enough to analyze with an electron microprobe. Most importantly, plagioclase crystallization was not observed in any of these experiments. Sodium, K and other elements found in enstatite meteorites were not included in the starting composition in order to simplify the composition. However, since these elements do not occur as important components in sulfides, this should not effect the results. Likewise, the Si/Mg ratio of our starting composition is higher than found in aubrites resulting in crystallization of SiO_2 in some experiments. Since SiO_2 is not abundant and does not incorporate REE, this should not affect the partition coefficients, even though it will cause the REE to become slightly concentrated in the remaining melt. The starting mixture consisted of oxides of Ca and Si, metallic Al and Mg and pyrite (FeS_2). Metallic Al and Mg were used as O getters to produce the low fO_2 of aubrite formation (log (fO_2) = −15 to −17; 3–5 log units below iron-wüstite at 1200 °C; Casanova, 1990). The starting material was a mixture of oxides, metals and sulfide rather than a homogeneous glass because producing a glass would have caused oxidation of the metals and loss of S from the pyrite. A CaO-SiO_2 glass could have been produced, but the high melting temperature of this material made this approach impractical.

TABLE 1. Experimental starting composition of our oldhamite partitioning experiments compared to natural aubrites on an oxygen-free basis.

	Aubrites*	Dickinson *et al.* (1990a)	Dickinson *et al.* (1990b,c)	Dickinson *et al.* (1991) and this work
Si	48.9	18.8	35.5	34.9
Mg	40.9	3.5	20.2	19.3
Al	0.9	17.2	6.1	6.1
Fe	7.4	45.0	8.6	9.1
S	0.9	5.5	9.9	10.4
Ca	1.1	5.9	19.8	20.2
Ni	–	4.1	–	–
	100.1	100.0	100.1	100.0

*Data from Watters and Prinz (1979).

Approximately 2 mg of each REE oxide was added to ~220 mg of starting material, producing ~1 wt% of each REE in the bulk melt. During electron microprobe analysis, REE were grouped (Eu-Gd, La-Ce, and Sm-Nd-Yb) to avoid analytical interferences resulting from overlapping x-ray lines (Drake and Weill, 1972). To test for Henry's law behavior, some samples were doped with ~0.25, 0.5, 2 and 4 wt% of each REE.

Rare-earth-element doped charges were thoroughly mixed, pressed into pellets, placed in alumina crucibles, dried overnight in an evacuated oven at 100 °C and sealed in evacuated silica tubes. During early experiments, it was not uncommon for the bottom of the silica tubes to crack shortly after being placed in the furnace. This appeared to be due to differential expansion during heating of the alumina crucible and silica tube. To alleviate this problem, silica wool was placed in the bottom of the silica tube, and the alumina crucible was placed on top of the silica wool. This allowed for a looser fit of the alumina crucible in the silica tube. Samples were suspended in air in the hot spot of vertical Deltech furnaces. Experimental temperatures were measured with Pt-$Pt_{90}Rh_{10}$ thermocouples calibrated against the melting point of Au. Temperatures are accurate to within ±5 °C.

Since the charges were run in sealed silica tubes, O fugacities could not be determined directly but were calculated from the phase relations present in the charges. The O fugacity of the charges was calculated considering equilibrium between Si in the metal and SiO_2 in the glass according to the reaction:

$$Si_{(kamacite)} + O_2 = SiO_{2\ (glass)}$$

We used the activity of Si in FeSi alloys determined by Sakao and Elliot (1975). Gibbs free energy values for SiO_2 were taken from Robie *et al.* (1978). As noted in Fogel *et al.* (1989), the activity of SiO_2 in the silicate glass is buffered by the presence or absence of forsterite, enstatite and free-SiO_2. Following the treatment of Fogel *et al.* (1989), we have done the calculations using two different activity coefficients for SiO_2 in the glass (0.5 and 1.0) . Oxygen fugacities calculated using both values are given in Table 2 for each experiment. These calculations suggest that the O fugacity is ~8 log units below the iron-wüstite buffer at these temperatures and is not significantly dependent on the activity of SiO_2 in the glass.

In order to examine the affects of fO_2 on partition coefficients, a series of charges were run with variable Mg/MgO ratios and a series with a variety of internal solid buffers (Cr, V, Al, Mg, Mn and C). The solid buffer was placed in a separate alumina crucible and then sealed in the silica tube with the sample. Buffers were examined after each experiment to check for the presence of both the metallic phase and the oxide as discussed later in this paper.

Run Thermal Histories

Experimental conditions and REE concentrations are given in Table 2. Samples were quenched by dropping them into an Al canister and blowing compressed air onto them until they were cool to the touch. We estimate that the samples were below the liquidus within a few seconds. Most samples were run at 1200 °C for two days. To test for the approach to equilibrium, Eu-Gd charges also were run at 1200 °C for one and seven days. To look at the effect of temperature on the partition coefficients, a few samples were run at 1300 °C for two days. Four Eu-Gd samples were held at 1200 °C for two days and then annealed at 800 °C for nine days to examine the affects of annealing on the partition coefficients.

Analyses of Samples

Samples were mounted in epoxy, sliced and polished for optical microscopy and electron microprobe analyses. To avoid hydration of the CaS, all samples were cut and polished using oil rather than water. In addition, all sections were stored in desiccators to minimize oldhamite decomposition. Samples were analyzed for major and rare earth elements using the Johnson Space Center Cameca Camebax automated electron microprobe, operating at an accelerating voltage of 20 kV and a beam current of 30 nA for all elements. Major element peaks and background were counted for 20 s and rare-earth-element peaks were counted for 60 s. All analyses were corrected for background, dead time, drift and matrix effects using the Cameca PAP routine.

Oldhamite grains were sometimes small and included within FeS, which presented significant analytical difficulties. Thus, oldhamite analyses that contained abnormally high abundances of Fe were not used in calculating partition coefficients. We used a fully focused beam for all analyses in this work to minimize beam overlap with other phases. We do not believe that the use of a fully focused beam significantly effects our interpretation of the partition coefficients, although this may have contributed to the low totals (90–95%) in the analyses of oldhamite. We believe the low totals are primarily due to oxidation and weathering of oldhamite in the terrestrial environment. Low totals occurred even though the samples were repolished just prior to the microprobe analyses, and similar analytical difficulties have been reported by others (*e.g.*, Larimer and Ganapathy, 1987; Wheelock *et al.*, 1994; Lodders, 1996a,b). Partition coefficients were based on the average composition of CaS and glass for each charge. In general, both phases were homogeneous within a single charge. Average oldhamite, glass and Fe metal compositions for 5–20 analyses of each phase within each charge are given in Appendix I. For sake of brevity, the number of analyses per phase per experimental charge and the standard deviations are not shown in Appendix I.

RESULTS

Petrography of Experimental Charges

The experimental charges produced here show a range of textures, mineralogies and mineral abundances. We can separate these experiments into three groups that show different textures or mineral abundances: 1300 °C, 1200 °C and 800 °C charges. Since the majority of our experiments were conducted at 1200 °C, we will provide a generalized description of these charges and note how the other groups differ. All of the charges are highly vesiculated, with vesicles occupying 50% or more of the charge, with either small (hundreds of micrometers) irregularly shaped vesicles, or large (multimillimeter) vesicles (Fig. 1a). The extreme vesicularity of some samples and the presence of sulfides lining vugs suggests that S volatilization occurred, and S was seen often lining the inside of the silica tube in which the alumina crucible containing the charge was sealed.

All 1200 °C charges contain some crystalline silicate phases. Small (tens of micrometers) enstatite crystals are distributed uniformly throughout the charges, whereas trace amounts of larger (hundreds of micrometers) semiequant or acicular SiO_2 crystals occur in patches. These crystalline phases are set in a matrix of glass. Only one of the three 1300 °C charges (TD-153) contains enstatite crystals, and none of the 1300 °C charges contain SiO_2. All 1300 °C charges also contain areas where micrometer-sized acicular quench crystals of enstatite have grown from the glass. The 800 °C annealing experiments (TD-205, -206, -215, -216) exhibit coarser-grained silicates, and all have crystallized diopside, although diopside is also observed in a few 1200 °C charges.

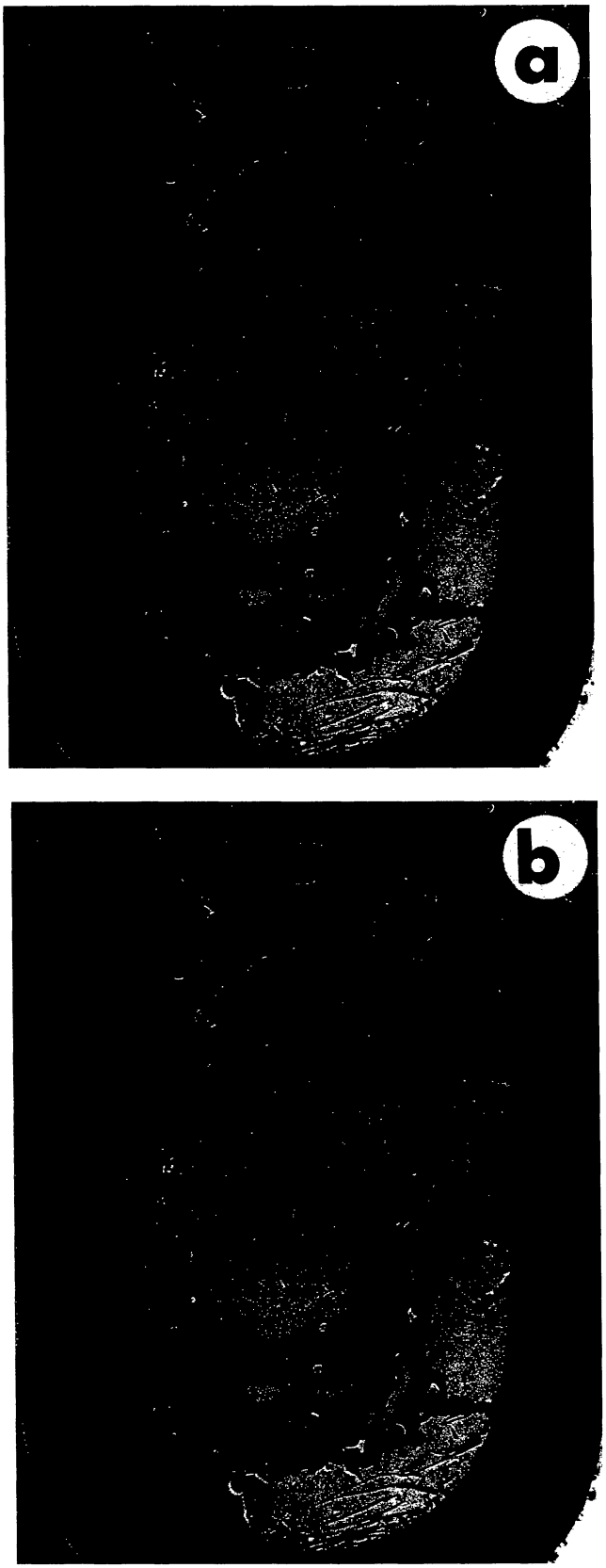

FIG. 1. Photomicrographs illustrating the textures of the experimental charges. (a) Experiment TD-183 (1200 °C Eu-Gd). The charge has a highly vesicular nature. Holes near bottom of sample represent areas drilled for oldhamite removal. The U-shaped alumina crucible is 1 cm in external diameter. (b) Reflected light photomicrograph of a composite oldhamite (O), troilite (T) and metal (M) particle in dark silicates from experiment TD-183. The curved oldhamite-troilite boundary suggests the existence of immiscible Ca-rich and Fe-rich sulfide liquids. The composite particle is 50 μm in diameter. This oldhamite particle was removed and examined by XRD techniques to confirm its crystalline nature.

TABLE 2. Summary of experimental conditions, calculated oxygen fugacities, oldhamite compositions, mineralogies and rare-earth-element partition coefficients.

Run No	153	158	171	154	183	196	197	198	199	200	164	157	208	209
Temp (°C)	1300	1300	1300	1200	1200	1200	1200	1200	1200	1200	1200	1200	1200	1200
Time (days)	2	2	2	2	2	2	2	2	2	2	7	2	2	2
REE level (wt%)	1	1	1	1	1	1	1	1	1	1	1	1	1	1
$-\log fO_2$ Si (a SiO2 = 1)	21.6	21.9	21.9	21.6	21.5	21.4	21.4	21.4	21.5	21.6	22	21.6	21.5	21.5
$-\log fO_2$ Si (a SiO2 = 0.5)	21.9	22.2	22.2	22	21.8	21.8	21.7	21.7	21.8	21.9	22.3	21.9	21.8	21.8
Oldhamite Composition														
X CaS	62.6	65.7	78.2	79.1	82.4	86.7	86.7	85.5	88.1	89.9	78	62.6	89.4	88.7
X MgS	28.9	31.1	20.4	17.3	12.4	6.9	9.3	6.9	8.5	6.9	20.4	26.8	5.9	5.5
X FeS	8.4	3.2	1.4	3.7	5.2	6.4	3.4	7.6	3.4	3.2	1.6	10.6	4.7	5.8
Phases present*		@	@											
SiO_2	–	–	–	+	+	+	+	+	+	+	+	+	+	+
FeS	–	–	–	–	+a	+a	+a	+a	+a	+a	–	–	+	+
Cpx	–	–	–	–	–	–	–	–	–	–	–	–	–	–
Other			Graphite								Graphite			
D CaS/Glass														
D La	—	—	0.3 (0.34)	—	—	—	—	—	—	—	—	—	—	—
D Ce	—	—	0.6 (0.07)	—	—	—	—	—	—	—	—	—	—	—
D Nd	—	1.2 (0.10)	—	—	—	—	—	—	—	—	—	2.2 (0.19)	0.8 (0.06)	0.7 (1.13)
D Sm	—	1.8 (0.08)	—	—	—	—	—	—	—	—	—	3.5 (0.31)	1.2 (0.05)	1.0 (1.40)
D Eu	1.2 (0.15)	—	—	1.7 (0.10)	2 (0.45)	1.9 (0.26)	1.9 (0.22)	1.9 (0.16)	1.9 (0.11)	2.0 (0.09)	1.6 (0.45)	—	—	—
D Gd	2.2 (0.18)	—	—	3.5 (0.19)	2.3 (0.41)	1.3 (0.19)	1.3 (0.24)	1.2 (0.23)	1.4 (0.19)	1.3 (0.17)	3.7 (1.02)	—	—	—
D Yb	—	2.9 (0.42)	—	—	—	—	—	—	—	—	—	4.4 (0.80)	0.7 (0.04)	0.6 (1.06)

Run No	218	219	155	211	212	178	162	161	179	180	185	176	177
Temp (°C)	1200	1200	1200	1200	1200	1200	1200	1200	1200	1200	1200	1200	1200
Time (days)	2	2	2	2	2	2	2	2	2	2	2	2	2
REE level (wt%)	1	1	1	1	1	0.25	0.5	2	4	0.25	4	0.25	4
$-\log fO_2$ Si (a SiO2 = 1)	22	22	21.8	21.4	21.5	21.6	21.8	21.8	21.6	21.6	21.7	21.6	21.7
$-\log fO_2$ Si (a SiO2 = 0.5)	22.3	22.3	22.1	21.7	21.8	21.9	22.1	22.1	21.9	21.9	22	21.9	22
Oldhamite Composition													
X CaS	88.4	89.7	67.8	89.4	87.2	73.7	74.7	81	85.1	84.1	79.8	75	87.4
X MgS	8.8	9.6	27.9	5.8	5.6	20.5	21.9	16.4	11.6	12.5	15.8	18.5	10.1
X FeS	2.8	0.7	4.7	4.8	7.1	5.8	3.3	2.6	3.2	3.4	4.4	6.5	2.5
Phases present*													
SiO_2	+	+	+	+	+	+	+	+	–	+	+	+	+
FeS	#	#	–	+	+	$	–	–	$	$	#	$	$
Cpx	–	–	–	+	+	–	–	–	–	–	–	–	–
D CaS/Glass													
D La	—	—	0.5 (0.04)	0.3 (0.28)	0.4 (0.29)	—	—	—	—	—	—	0.6 (0.15)	0.3 (0.02)
D Ce	—	—	1.0 (0.06)	0.5 (0.26)	0.5 (0.32)	—	—	—	—	—	—	1.2 (0.22)	0.6 (0.05)
D Nd	1.0 (0.12)	1.0 (0.06)	—	—	—	—	—	—	—	1.8 (0.61)	1.4 (0.09)	—	—
D Sm	1.3 (0.11)	1.3 (0.6)	—	—	—	—	—	—	—	2.7 (0.68)	2.0 (0.08)	—	—
D Eu	—	—	—	—	—	1.3 (0.15)	1.3 (0.32)	1.8 (0.31)	2.1 (0.10)	—	—	—	—
D Gd	—	—	—	—	—	4.6 (1.17)	4.1 (1.05)	2.8 (0.92)	1.7 (0.02)	—	—	—	—
D Yb	3.1 (0.24)	3.1 (0.26)	—	—	—	—	—	—	—	3.5 (0.81)	2.6 (0.10)	—	—

TABLE 2. *Continued.*

Run No	173	174	225	228	229	230	231	232	205	205	206	206	215	216
Temp (°C)	1200	1200	1200	1200	1200	1200	1200	1200	1200/800	1200/800	1200/800	1200/800	1200/800	1200/800
Time (days)	2	2	2	2	2	2	2	2	2/9	2/9	2/9	2/9	2/9	2/9
REE level (wt%)	1	1	1	1	1	1	1	1	1	1	1	1	1	1
Buffer	0.25 MgO	0.5 MgO	Cr	Mg	C	Al	Mn	V						
$-\log fO_2$ Si (a SiO2 = 1)	21.4	21.5	21.5	22.6	None	None	None	21.5	21.6	—	21.6	—	21.3	21.4
$-\log fO_2$ Si (a SiO2 = 0.5)	21.7	21.8	21.8	22.9	None	None	None	21.8	21.9	—	21.9	—	21.6	21.7
Oldhamite Composition									Not in FeS	In FeS	Not in FeS	In FeS		
X CaS	86.2	88.1	90.8	88.7	89.9	N/A	N/A	82	96.2	95.5	96.6	95.7	96.1	96.4
X MgS	9.8	7.6	5.9	10.6	6.3	N/A	N/A	10.5	1	1	1	0.8	1.6	1.1
X FeS	4	4.3	3.3	0.7	3.8	N/A	N/A	7.5	2.8	3.5	2.4	3.5	2.3	2.5
Phases present*					†	†‡	§‡							
SiO_2	+	+	–	–	+	–	–	–	+	—	+	—	+	+
FeS	+	+	–	–	+	–	–	–	+	—	+	—	+	+
Cpx	–	–	–	–	–	+	–	+	+	—	+	—	+	+
D CaS/Glass														
D Eu	1.9 (0.22)	2.0 (0.26)	1.6 (0.66)	2.0 (0.25)	2.7 (1.87)	N/A	N/A	1.9 (0.61)	2.7 (1.87)	16.1 (2.93)	2.3 (1.20)	9.6 (1.80)	2.9 (1.45)	4.1 (2.50)
D Gd	1.9 (0.25)	2.0 (0.26)	0.6 (0.27)	1.1 (0.30)	1.0 (0.55)	N/A	N/A	0.7 (0.51)	0.8 (0.51)	3.3 (0.43)	0.6 (0.26)	1.9 (0.26)	1.0 (0.44)	0.8 (0.61)

*Charges contain glass, enstatite, metal, and oldhamite unless otherwise noted.
†No metal present.
‡No CaS present.
§Sample leaked.
#Small grains in metal.
$Rims on metal.
@No enstatite present.
– = not present, + = present, +a = abundant, — = no data.

Opaque mineral textures are complex, depending in large part on the phases present and their relative abundances. Many charges contain only metallic Fe and oldhamite as nonsilicate phases; all charges utilized in this study contain these two phases because oldhamite partitioning was the goal of this study and because the composition of metallic Fe was an essential factor in determining the O fugacity. Oldhamite observed in polished thin section is red-brown in transmitted light. Confirmation that CaS is crystalline oldhamite is provided by x-ray diffraction analysis (M. Zolensky, pers. comm., 1995) that produced d-spacings similar to those in previously studied synthetic (JCPDF 8-464) and natural oldhamites (Wheelock *et al.*, 1994). In the oldhamite-metallic Fe charges, metallic Fe forms semiequant particles and oldhamite occurs both in contact with the metallic Fe and in the silicate matrix as particles ranging in size from a few micrometers to tens of micrometers. Intergrowths of these two phases are not observed. In the presence of troilite, oldhamite occurs as rounded isolated particles 1–100 μm in diameter, as partial linings on vesicles within the charge and as particles tens of micrometers in size separated from troilite by curved boundaries (Fig. 1b). The textural relationship of troilite and oldhamite strongly suggests that the Fe-rich and Ca-Mg-rich sulfide melts were immiscible, as also observed by Jones and Boynton (1983). Troilite-metal intergrowths are also common, including a fine-scale intergrowth typical of the quenching of FeS melts. Larger (tens of micrometers), rounded metal particles are often partially to completely enveloped in troilite. Other highly reduced sulfides, which are common in aubrites, (*e.g.*, daubreelite, alabandite) were not observed in these charges because the starting composition did not contain Cr or Mn.

Rare-earth-element Partitioning

The major focus of this study was to determine the partitioning of REEs between oldhamite and silicate glass. In our experiments, partition coefficients may be effected by as many as six factors: attainment of equilibrium, composition of the oldhamite (note that our experiments all used a single starting composition and we did not evaluate the possible influence of bulk composition on partitioning), temperature of melting, O fugacity, minor element abundances (Henry's Law) and low-temperature annealing. In this section, we evaluate the possible influences of each of these.

Equilibrium, Reproducibility and Analytical Uncertainties– The vast majority of our experiments were run for two days but did not experience significant instability in sealed silica tubes, even with run times as long as seven days. We were not able to run reversals of the kind commonly employed in solid-liquid partitioning experiments. Instead, we have employed the classical technique of the approach to equilibrium with time by running 1200 °C Eu-Gd doped experiments for one (TD-200), two (TD-154) and seven (TD-164) days (Table 3). As we show in the next section, partition coefficients are strongly dependent on oldhamite composition and, thus, attainment of equilibrium must be evaluated in experiments that produced oldhamite of similar composition. Sample TD-164 produced oldhamite (78 mol% CaS) of comparable major element composition to experiment TD-154 (79 mol% CaS), which was held at 1200 °C for two days. The CaS in TD-200 (one day) was more Ca-rich (90 mol% CaS) than either the two or seven day experiments and is comparable to TD-196–199, which were run for two days each. The partition coefficients (D) did not differ significantly be-

tween TD-154 and TD-164 and between TD-196–199 and TD-200, thus attesting to the attainment of equilibrium within the typical two day run time. In actuality, equilibrium appears to have been reached within one day.

We also performed replicate experiments in order to test the reproducibility of our techniques. We ran multiple experiments at 1200 °C for two days with 1 wt% of each REE for the La-Ce charges (three replicates), Sm-Nd-Yb charges (five replicates) and Eu-Gd charges (six replicates). These charges contained oldhamite with 63–90 mol% CaS. Again, we must evaluate the reproducibility of our partition coefficients by considering experiments that produced oldhamite of similar compositions. To do this, we consider only those 1200 °C experiments that were doped with 1 wt% levels of each REE and that produced oldhamite with 85–90% CaS. Experiments TD-211 and TD-212 produced oldhamite of 87–89% CaS and reproducible partition coefficients for La (0.3, 0.4) and Ce (0.5, 0.5). Experiments TD-196, 197, 198 and 199 (86–88% CaS) also yielded reproducible partition coefficients for Eu (all 1.9) and Gd (1.2, 1.3, 1.3, 1.4). Experiments TD-208, 209, 218 and 219 (89% CaS) yielded reproducible partition coefficients for Nd (of 0.7, 0.8, 1.0, 1.0) and Sm (of 1.0, 1.2, 1.3, 1.3) but not for Yb (of 0.6, 0.7, 3.1, 3.1). An important exception to this consistency comes in examining Yb partition coefficients for experiments TD-218 and TD-219. The choice of D_{Yb} between these two sets of experiments drastically alters the partition coefficient pattern. Samples TD-218 and TD-219 differ petrographically from the others as well, containing only minor troilite (finely interspersed in Fe metal) with abundant oldhamite and metal with very high concentrations of Si (16 wt%). Since TD-208 and 209 appear to more closely replicate oldhamite crystallization in aubrites (*e.g.*, abundant troilite, lower Si in metal), we favor use of the lower D_{Yb} from TD-208 and 209. We note that both sets of experiments satisfy our minimum criteria for a successful experiment as listed earlier. Among the REEs, Yb partitioning may be particularly sensitive to some factor that we do not fully understand.

In calculating partition coefficients, we utilized average glass and CaS compositions (Appendix 1) for 5–20 analyses of each phase within each experimental charge. The standard deviation of the average of the analyses is commonly taken as a measure of the analytical uncertainty (*e.g.*, Hillgren *et al.*, 1996). Since the phases are homogeneous, the variability of the measurement should represent the error inherent in each individual analysis based on counting statistics and represents how well we know the concentration of a given element. The uncertainties shown in Table 2 and plotted in Figs. 2b, 4 and 5 are based on this type of error analyses.

Another measure of the analytical uncertainty can be garnered by comparing partition coefficients from replicate experiments. Again, we consider only those 1200 °C experiments doped with 1 wt% levels of each REE and that produced oldhamite with 85–90% CaS. Using this method, the experiments utilized and associated errors are as follows: La (#211, 212; 0.07), Ce (#211, 212; 0.0), Nd (#208, 209, 218, 219; 0.15), Sm (#208, 209, 218, 219; 0.17), Eu (#196–200; 0.0), Gd (#196–200; 0.07) and Yb (#208, 209; 0.21). Uncertainties based on the standard deviations of the microprobe analyses are typically, but not universally, larger than those based on reproducibility of the experiments.

TABLE 3. Comparison of one, two and seven day charges as a test for attainment of equilibrium.

Sample	Duration	CaS%	D_{Eu}	D_{Gd}
164	seven days	78	1.6	3.7
154	two days	79	1.7	3.5
196–199	two days	88	1.9	1.3
200	one day	90	2.0	1.3

Oldhamite Composition–Oldhamite in our charges ranged in composition from 63–90 mol% CaS. Partitioning of at least some of the REEs is dependent on oldhamite composition (Table 4 and Fig. 2a). Lanthanum and Ce exhibit relatively small variations in the absolute magnitude of their partition coefficients but large relative variation. Oldhamite compositions in experiments doped with La and Ce vary from 67–89% CaS, with D_{La} varying from 0.5–0.3 (a factor of 1.6 relative) and D_{Ce} from 1.0–0.5 (a factor of 2). Experiments doped with Nd, Sm and Yb varied in oldhamite composition from 63–90% CaS. All three elements show significant variability in both absolute and relative $D_{CaS/Glass}$, with Nd ranging from 2.2–0.7 (factor of 3), Sm, from 3.5–1 (factor of 3.5) and Yb, from 4.4–0.6 (factor of 7). Experiments doped with Eu and Gd exhibit a smaller range of oldhamite composition from 79–90% CaS. Europium exhibits essentially no dependence on composition over this smaller range, while Gd shows an exceptionally large dependence on composition, with D_{Gd} varying from 3.5–1.3. Thus, partition coefficients of Nd, Sm, Gd and Yb are highly dependent on oldhamite composition, while La, Ce and Eu show relatively small compositional dependencies, particularly in the absolute value of partition coefficient. It also should be noted that the dependence of partition coefficients on oldhamite composition tends to be minimal at oldhamite compositions >~85% CaS. Most natural oldhamites are >85% CaS.

The dependence of partition coefficients on oldhamite composition yields different distribution coefficient patterns depending on the composition of the oldhamite (Fig. 2b). With the exception of La and Ce, differences in partition coefficients as a function of oldhamite composition are greater than the 1σ error bars. The partition coefficient pattern for the 1200 °C experiments with Ca-poor (63–79% CaS) oldhamite is light rare-earth-element (LREE) depleted and heavy rare-earth-element (HREE) enriched, with D_{La} of 0.5 and D_{Yb} of 4.4. This pattern, which also exhibits a prominent negative Eu anomaly, was illustrated by Dickinson *et al.* (1991). In contrast, the partition coefficient pattern for the 1200 °C experiments with Ca-rich (88–89% CaS) oldhamite is bow shaped, with D_{La} of 0.4 and D_{Yb} of 0.7. This pattern exhibits a positive Eu anomaly. If one were to accept the higher D_{Yb} values (TD-218 and 219) as discussed above, the Ca-rich oldhamite pattern at 1200 °C would be LREE depleted, HREE enriched and have a positive Eu anomaly. Thus, not only the absolute abundances, but also the shape of the REE pattern

TABLE 4. Partition coefficients in 1200 °C charges to illustrate the dependence of partitioning on oldhamite composition.

Sample	CaS %	D_{La}	D_{Ce}	D_{Nd}	D_{Sm}	D_{Eu}	D_{Gd}	D_{Yb}
155	67	0.5	1.0	–	–	–	–	–
212	87	0.4	0.5	–	–	–	–	–
211	89	0.3	0.5	–	–	–	–	–
157	63	–	–	2.2	3.5	–	–	4.4
208	89	–	–	0.8	1.2	–	–	0.7
209	89	–	–	0.7	1.0	–	–	0.6
154	79	–	–	–	–	1.7	3.5	–
183	82	–	–	–	–	2.0	2.3	–
198	86	–	–	–	–	1.9	1.2	–
196	87	–	–	–	–	1.9	1.3	–
197	87	–	–	–	–	1.9	1.3	–
199	88	–	–	–	–	1.9	1.4	–

and the nature of the Eu anomaly of crystallizing oldhamite can be influenced by the composition of the oldhamite. Although the sign of the Eu anomaly varies with oldhamite composition, this is entirely due to differences in the magnitude of the Sm and Gd partition coefficients. Contrary to the assertion of Lodders (1995, 1996a,b), who argued that the Eu partitioning is dependent on oldhamite composition, our experiments indicate Eu partitioning is insensitive to oldhamite composition.

Temperature of Melting–Although most of our experiments were conducted at 1200 °C, three experiments (TD-153, -158 and -171) were run at 1300 °C (one for each group of REE; Table 5). The oldhamites in these experiments were generally Ca-poor (63–78% CaS) and had variable compositions between the three experiments. Thus, we must consider the possible influence of oldhamite composition before asserting a temperature dependence for partitioning. As discussed above, partitioning of Gd, Yb, Sm and Nd at 1200 °C all show strong dependence on oldhamite composition, while partitioning of Eu, Ce and La do not. In Fig. 3a, we plot the 1300 °C partition coefficients against oldhamite composition (mol% CaS). Partition coefficients for Gd, Yb, Sm and Nd all plot significantly away from the compositional dependence lines based on the 1200 °C data. This suggests that differences in partition coefficients between the 1200 °C and 1300 °C data are not due to compositional differences but rather result from a real temperature dependence.

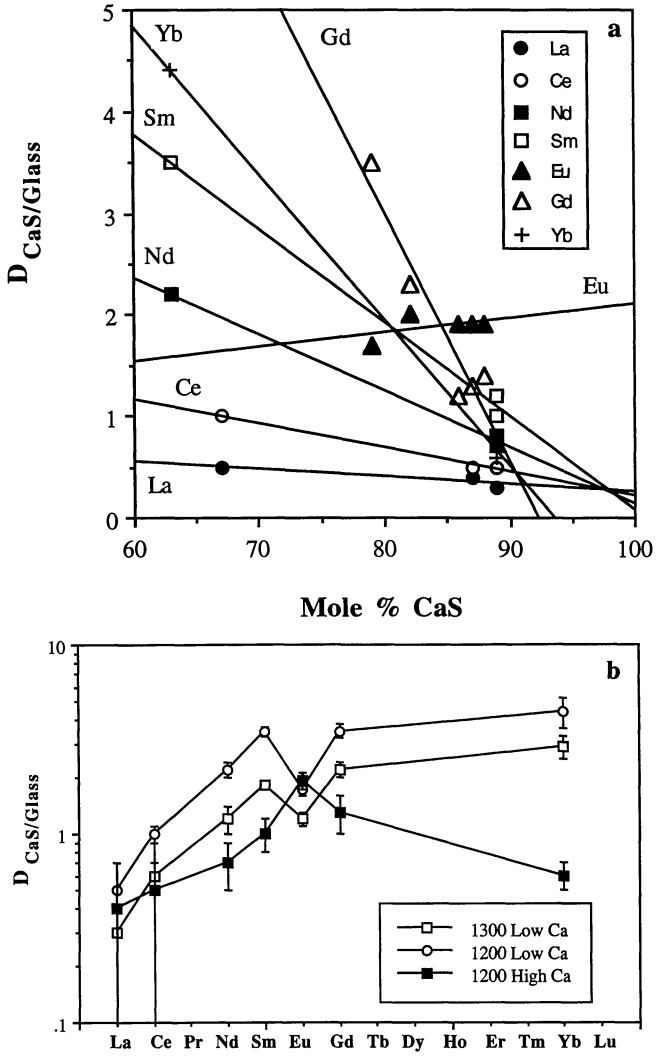

FIG. 2. Variation of partition coefficients (D) with oldhamite composition and temperature. (a) Data for 1200 °C experiments with 1% doping levels for each REE. Lines represent best fits to the data. Partition coefficients for Nd, Sm, Gd and Yb are highly dependent on oldhamite composition, whereas La, Ce and Eu show relatively small compositional dependencies. Partition coefficients are independent of oldhamite composition at compositions >85% CaS. (b) Partition coefficient patterns for 1200 °C and 1300 °C experiments that produced Ca-poor (63–79% CaS) oldhamite. Comparison of these patterns demonstrates the increase in partition coefficients with decreasing temperatures. Also shown are the partition coefficients for Ca-rich (88–89% CaS) oldhamite in the 1200 °C experiments. This pattern differs dramatically from the others, illustrating the influence of oldhamite composition on partitioning. Error bars are based on the standard deviation of the microprobe analyses of both the glass and sulfide, as discussed in the text.

We can further examine this temperature dependence by comparing the 1300 °C experiments (TD-153, -158 and -171; 63–78% CaS) with 1200 °C experiments of comparable composition (TD-154, -155 and -157; 63–79% CaS). Data from these two sets of experiments are listed in Table 5 and illustrated in Fig. 2b. These curves are essentially identical in their form, with LREE depletion, HREE enrichment and a prominent negative Eu anomaly. Partition coefficients for the 1200 °C experiment are factors of 1.4–1.9× higher than those of the 1300 °C experiment, which suggests that preferential incorporation of REE into oldhamite increases with decreasing temperature. With the exception of La, partition coefficient variation between 1200 °C and 1300 °C is greater than the errors associated with the measurements.

Minor Element Abundance (Henry's Law)–The experiments discussed to this point were all doped with REE at levels of ~1 wt% for each REE oxide. We also conducted experiments doped at 0.25–4 wt% to test for ideal behavior of trace-element partitioning. Lanthanum-cerium and Sm-Nd-Yb experiments were doped at 0.25 and 4 wt% levels, whereas Eu-Gd experiments were doped at 0.25, 0.5, 2 and 4 wt% for each REE oxide. This range of concentrations should allow us to test ideal behavior and partitioning. Results of these experiments are listed in Table 6 and illustrated in Fig. 3b. We have shown in an earlier section that partition coefficients are strongly dependent on oldhamite composition for some elements. Thus, in those cases where the composition of the oldhamite varies with REE concentration, we must examine first the possible influence of oldhamite composition before concluding that nonideal behavior has occurred.

Partition coefficients for La and Ce vary by a factor of two between the 0.25 and 4 wt% doped charges. In addition, the composition of the oldhamite varies between these two charges. Thus, we must consider the possible influence of oldhamite composition on partitioning. For La, the 0.25% charge (75% CaS) and the 4% charge (87% CaS) fall close to or on the line of compositional dependence *vs.* partition coefficient defined by the 1% charges (Fig. 3b).

TABLE 5. Distribution coefficients from 1200 °C and 1300 °C experiments with CaS-poor oldhamite and 1200 °C experiments with CaS-rich oldhamite to illustrate influence of temperature and composition.

Sample	T (°C)	CaS%	D_{La}	D_{Ce}	D_{Nd}	D_{Sm}	D_{Eu}	D_{Gd}	D_{Yb}
153	1300	63	–	–	–	–	1.2	2.2	–
158	1300	66	–	–	1.2	1.8	–	–	2.9
171	1300	78	0.3	0.6	–	–	–	–	–
154	1200	79	–	–	–	–	1.7	3.5	–
157	1200	63	–	–	2.2	3.5	–	–	4.4
155	1200	67	0.5	1.0	–	–	–	–	–
196–199	1200	88	–	–	–	–	1.9	1.3	–
208/209	1200	89	–	–	0.8	1.1	–	–	0.7
211/22	1200	88	0.4	0.5	–	–	–	–	–

Partition coefficients for Ce fall slightly above the 1% compositional dependence line for both 0.25 and 4 wt% doped charges, although the difference between these charges is comparable to that expected from the 1% experiments. Variations in partition coefficients for 0.25 and 4 wt% La-Ce charges appear to be due to oldhamite compositional dependence and, thus, La and Ce behave ideally over this range of REE concentration.

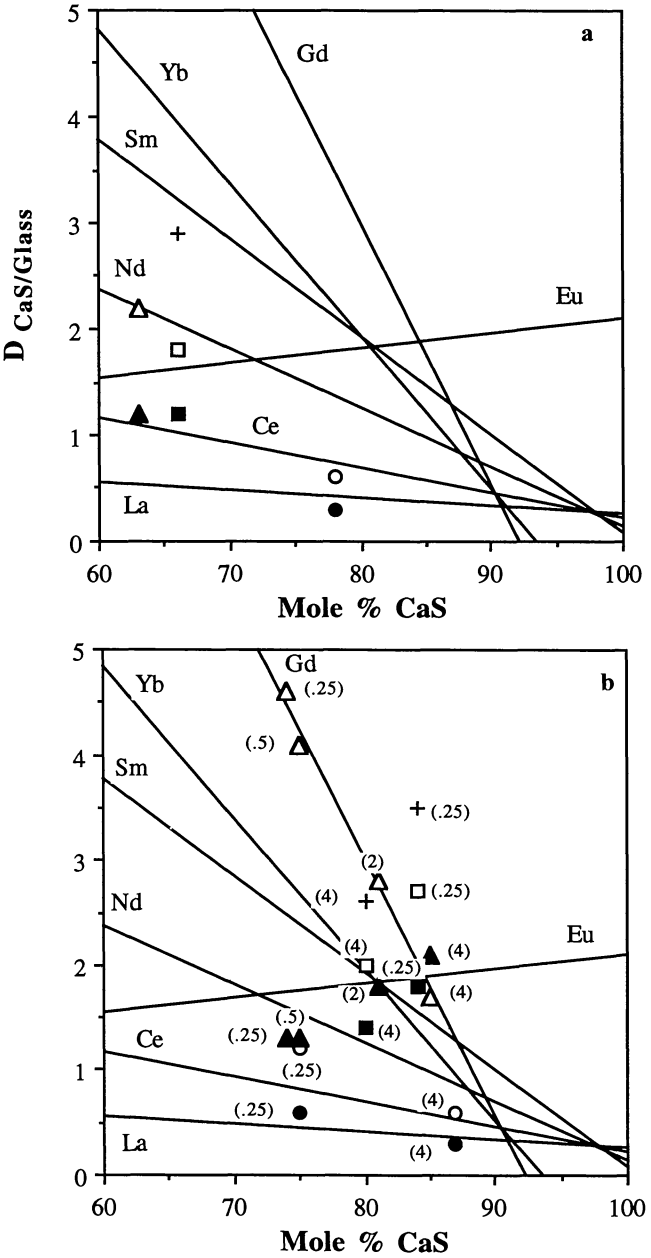

FIG. 3. Partition coefficients *vs.* oldhamite composition. (a) Data for 1300 °C experiments with compositional dependence lines from Fig. 2a. Partition coefficients for Gd, Yb, Sm and Nd all plot significantly away from the 1200 °C lines, which suggests that partition coefficients are dependent on temperature and not just on oldhamite composition. (b) Data for 1200 °C experiments with variable REE levels (0.25, 0.5, 3 and 4 wt% of each REE oxide) with compositional dependence lines from Fig. 2a. Variations in La, Ce, Eu and Gd appear to be dependent on compositional differences and, thus, behave ideally. The partition coefficients for Nd, Sm and Yb vary independently of the compositional dependence. The significance of this variation is discussed in the text.

Partitioning experiments at 0.25, 0.5, 2 and 4 wt% levels for Eu show a slight increase in D_{Eu} (1.3–2.1) with both REE concentration and oldhamite composition, while D_{Gd} decreases dramatically (4.6–1.7) with both REE concentration and oldhamite composition. Both of these trends appear to mirror compositional trends defined by the 1% level experiments (Fig. 3b). Partition coefficients for Eu plot around the Eu 1% compositional dependence, with those at lower concentrations plotting slightly below the line. It should be noted that the 0.25 and 0.5 wt% experiments produced slightly less calcic oldhamite (74–75% CaS) than the 1 wt% experiments (79% CaS). In addition, some scatter existed in the 1% data (Fig. 2a). Gadolinium partition coefficients plot closer to the 1 wt% Gd compositional dependence line and also extend to less calcic oldhamite compositions. Thus, Gd and Eu also appear to behave ideally.

The variation in the partitioning behavior of Nd, Sm and Yb with concentration is less clear. Experiments run at 4 wt% doping levels fall reasonably close to the 1 wt% compositional dependence lines (Fig. 3b). In contrast, partition coefficients at 0.25 wt% doping levels fall well above the 1 wt% lines. It is somewhat surprising that the 4% experiments fall close to the 1 wt% lines, while the 0.25 wt% experiments deviate significantly. Normally, one would expect the reverse, since partitioning should become less ideal with increasing concentration. It is possible to argue that the 0.25 wt% experiments represent ideal behavior, with the 1 wt% and 4 wt% experiments behaving nonideally. However, we suggest that the 0.25 wt% experiment is, in fact, in error. Experiment TD-180 may not have attained equilibrium. We identified distinct metal particles and different regions within a single metal particle with a wide range of Si concentrations (6.5–32.6 wt%), which suggests that the charge was not homogenized with respect to fO_2. This was the only experiment in which metal with variable Si composition was observed. This lack of equilibrium suggests that TD-180 may not accurately reflect equilibrium REE partitioning. We believe the agreement between the 1 wt% and 4 wt% experiments indicates that REE partitioning was near ideal in our 1 wt% Nd-Sm-Yb doped charges.

Oxygen Fugacities–In order to determine the effect of O fugacity on the partition coefficients, we conducted two sets of experiments using Eu-Gd doped charges. Europium was specifically investigated since it might be particularly sensitive to changes in oxidation state. Results of these experiments are shown in Table 7. In the first set of experiments, the ratio of MgO to metallic Mg in the starting composition varied from 0 to 0.5. It should be noted that on

TABLE 6. Experiments doped with variable wt% levels of rare-earth-element oxides to check for Henry's Law behavior.

wt%	0.25	0.5	1		2	4
D_{La}	0.6	–	0.5	0.3	–	0.3
D_{Ce}	1.2	–	1.0	0.5	–	0.6
CaS%	75	–	68	89	–	87
Charge	176	–	155	211	–	177
D_{Nd}	1.8	–	2.2	0.8	–	1.4
D_{Sm}	2.7	–	3.5	1.2	–	2.0
D_{Yb}	3.5	–	4.4	0.7	–	2.6
CaS%	84	–	63	89	–	80
Charge	180	–	157	208	–	185
D_{Eu}	1.3	1.3	1.7		1.8	2.1
D_{Gd}	4.6	4.1	3.5		2.8	1.7
CaS%	74	75	79		81	85
Charge	178	162	154		161	179

an O free basis (Table 1), this does not change the bulk composition of the starting material. A second set of experiments were run with a variety of internal solid buffers (Cr, V, Al, Mg, Mn and C). The solid buffer was placed in a separate alumina crucible that had slots in the top to allow vapor transfer and sealed in the silica tube with the sample. All of the charges were run at 1200 °C for 48 h. Buffers were examined after each experiment to check for the presence of both the metal and oxide phases. Oxygen fugacities of the solid buffers at 1200 °C were calculated from thermodynamic data given by Robie *et al.* (1978). Calculated O fugacities of these buffers ranged from log fO_2 of –29.9 (Mg-MgO) to –17.3 (C-CO). Note that iron-wüstite is log fO_2 = –12 at 1200 °C. Two of the experiments were not usable for this study since they contained no oldhamite. The Mn buffered charge appears to have leaked, oxidizing all of the Mn, while the Al buffered charge contained no sulfides, which suggests total volatilization of S. The top of the sealed silica tube contained a fine-grained, dark material of undetermined composition that may have contained the volatilized S. In addition, the alumina crucible was severely degraded.

The charges with variable MgO/Mg ratios all produced comparable oldhamite compositions (86–88% CaS) and O fugacities (–21.4 to –21.8). Partition coefficients for Eu were quite similar (1.9–2.0). The D_{Gd} ranges from 1.3–2.0. The extremely narrow range of calculated O fugacities, however, suggests that this variation is not dependent on O fugacity. The calculated O fugacities of the internal solid buffers (Mg, V, Cr, C) would yield a considerable range of –log fO_2 from –29.9 to –17.3 at 1200 °C. However, –log fO_2 determined from phase compositions showed a considerably smaller range (–21.5 to –22.9). We suggest that differences between ideal and calculated fO_2 resulted from incomplete equilibrium between the charges and buffers. In the case of the Mg buffer, the ideal fO_2 (–29.9) is much more reducing than the measured fO_2 (–22.6 to –22.9). Examination of this charge suggests that Mg was completely oxidized during the experiment and, thus, the ideal fO_2 was never approached. Over the relatively narrow range of fO_2 actually achieved in these four buffering experiments, no correlation between fO_2 and D_{Eu} or D_{Gd} is observed.

We find no dependence of partition coefficients on O fugacity for Eu and Gd in either the variable Mg/MgO experiments or in the experiments with internal solid buffers. We recognize that the range of O fugacities investigated was small but also recognize that the crystallization of oldhamite is restricted to very reducing conditions similar to those of these experiments.

TABLE 7. Experiments that attempted to vary fO_2 by varying the MgO/Mg ratio of the starting material or including a solid buffer.

	Experiment	CaS%	–log fO_2 Theoretical	–log fO_2 Phases	D_{Eu}	D_{Gd}
Variable MgO/ Mg Ratios						
0	196	86.7	–	21.4–21.8	1.9	1.3
0.25	173	86.2	–	21.4–21.7	1.9	1.9
0.5	174	88.1	–	21.5–21.8	2.0	2.0
Solid Buffer						
Mg-MgO	228	88.7	–29.9	22.6–22.9	2.0	1.1
Al-Al_2O_3	230	–	–28.1	–*	–	–
V-V_2O_3	232	82.0	–20.0	21.5–21.8	1.9	0.7
Mn-MnO	231	–	–19.4	–*	–	–
Cr-Cr_2O_3	225	90.8	–17.6	21.5–21.8	1.6	0.6
C-CO	229	89.9	–17.3	–†	2.7	1.0

Calculated fO_2 of solid buffers at 1200 °C from data of Robie *et al.* (1978) and calcuated fO_2 for all charges based on the amount of Si in the metal.
*No oldhamite present.
†No metal present.

Annealing Experiment–We ran four Eu-Gd doped charges (TD-205, -206, -235 and -216) at 1200 °C for two days and then annealed them at 800 °C for nine days to evaluate the possible influence of annealing on REE partitioning. All of these charges contained oldhamite much more calcic (95–97% CaS) than those produced in experiments that were not annealed (87% CaS). We do not believe these compositional differences effected the partition coefficients, since partition coefficients do not vary significantly with composition at oldhamite compositions >85% CaS (Fig. 2a). The Eu and Gd partition coefficients and oldhamite compositions for the annealed charges are given in Table 8. Experiments TD-205 and -206 contained two occurrences of oldhamite: one enclosed within or associated with FeS and the other not associated with FeS. Grains not associated with FeS generally give partition coefficients similar to those in the nonannealed experiments (Fig. 4). The partition coefficients for Eu and Gd are significantly larger for the oldhamite grains associated with FeS. It is interesting to note that D_{Eu} and D_{Gd} for the 800 °C annealed charges are higher than for the 1200 °C charges. This trend of increasing partition coefficient with decreasing temperature is the same trend we saw from 1300 °C to 1200 °C.

Summary of REE Partitioning–Our experiments reveal several important features of REE partitioning between oldhamite and silicate glass. We have already discussed the dependence of partitioning on several experimental variables and briefly summarize these features here. Rare-earth-element partitioning in oldhamite shows considerable dependence on oldhamite compositions, although this dependence appears to be minimal at oldhamite compositions >85% CaS. Partitioning also shows a strong dependence on temperature. Experiments at comparable oldhamite composition show that the 1200 °C charges have higher partition coefficients than those at 1300 °C. In addition, 1200 °C experiments annealed at 800 °C for nine days contain some oldhamite grains that are significantly enriched in REEs compared to those that were not annealed. Partitioning of REEs in oldhamite does not appear to be dependent on the absolute abundances of the REEs and, thus, ideal behavior is observed. There is no measurable dependence of partitioning on O fugacity, although our experiments were run over the relatively narrow range of fO_2 in which oldhamite is a stable phase.

A second important feature of our set of experiments that we have not discussed previously is the general magnitude of the partition coefficients. Wheelock *et al.* (1994) inferred that oldhamite/silicate partition coefficients in natural systems should be on the order of 100–1000, based on ion microprobe data of naturally occurring oldhamite in Norton County and comparison with the bulk REE

TABLE 8. Comparison of 1200 °C charges with and without seven day annealing. Annealed charges TD-205 and 206 contained oldhamites of different rare-earth-element concentration.

Sample	Occurrence	CaS%	D_{Eu}	D_{Gd}
196		86.7	1.9	1.3
205	without FeS	96.2	2.7	0.8
205	with FeS	95.5	16.1	3.3
206	without FeS	96.6	2.3	0.6
206	with FeS	95.7	9.6	1.9
215		96.1	2.9	1.0
216		96.4	4.1	0.8

inventory of this aubrite. We note that our experiments, regardless of oldhamite composition, time or temperature, all yield REE partition coefficients <20. With the exception of Eu partitioning in the annealing experiments, all partition coefficients are <5. We also note that partition coefficients for 1200 °C calcic oldhamite experiments yields D > 1 for Sm, Eu and Gd and D < 1 for La, Ce, Nd and Yb. Thus, REEs differ in their preference for incorporation into oldhamite compared to silicate glass.

COMPARISON WITH LITERATURE DATA

As noted in the introduction, discussion in the literature on the partitioning of REE between oldhamite and silicates is rare. In this section, we briefly compare our results to the results of Jones and Boynton (1983), which utilized a eucritic starting composition, and more fully compare our results to those of Lodders *et al.* (1990) and Lodders (1995, 1996a,b), who also used an enstatite meteorite composition (Table 9).

Jones and Boynton (1983) report partition coefficients for La, Gd, and Lu between (Mg,Ca)-rich sulfide liquid and silicate liquid using a eucritic starting composition and run times of 1–4 h. They produced early crystallizing Al-rich phases (*e.g.*, plagioclase, corundum and spinel) and, thus, did not simulate the crystallization of aubrites. In addition, phases were very heterogeneously distributed, and equilibrium may not have been attained. They report D_{La} of 0.4, D_{Gd} of 12 and D_{Lu} of 24 at 1200 °C, yielding a (Mg,Ca)-rich sulfide liquid/silicate liquid partition coefficient pattern that is LREE depleted and HREE enriched. They did not examine partitioning of Eu and, thus, no information about an Eu anomaly is known. They also examined partitioning at 1150 °C and 1250 °C and observed increasing sulfide liquid/silicate liquid partition coefficients with decreasing temperature. In addition, at 1150 °C, they produced oldhamite enriched in LREE relative to the (Ca,Mg)-rich sulfide liquid from which it grew.

It should be noted that the experiments of Jones and Boynton (1983) reported (Mg,Ca)-rich sulfide liquid at 1200 °C and not crystalline oldhamite. These authors did not report the composition of the oldhamite or the (Mg,Ca)-rich sulfide liquid. In addition, these authors utilized a different bulk composition and run times than we used. Despite these potentially significant differences, several of the observations made by Jones and Boynton (1983) are consistent with our observations. The pattern of LREE depletion and HREE enrichment in their Mg-rich sulfide liquid is similar to the pattern that we observed in our 1200 °C CaS/silicate liquid experiments that produced Ca-poor oldhamite (Fig. 2b). We also observed the trend of increasing partition coefficients with decreasing temperature. Our D_{La} (0.3–0.5) for Ca-poor and Ca-rich oldhamite is similar to that reported (0.4) by Jones and Boynton (1983). The Gd and Yb partition coefficients observed by Jones and Boynton (1983) are up to 20× higher than observed in our experiments. As shown in Fig. 2a, our data show a strong dependence of Gd and Yb partitioning on oldhamite composition. Therefore, the difference in Gd and Yb partition coefficients between Jones and Boynton (1983) and this work may be due to compositional differences. However, we do note that even these experiments yielded partition coefficients <25. As in our experiments, this is far below the inferred partition coefficients of 100–1000 by Wheelock *et al.* (1994). Finally, although we have not discussed these in detail, the early experiments of Dickinson *et al.* (1990a,b,c) also utilized a eucritic composition. These experiments produced patterns of LREE depletion and HREE enrichment but with partition coefficients <10. Thus, it appears that both our aubritic composition and these eucritic compositions produce partition coefficients considerably less than those inferred from natural samples, although these studies differ in experimental detail.

The technique used by Lodders *et al.* (1990) and Lodders (1995, 1996a,b) to determine REE partitioning differs dramatically from our work as discussed below, and we will discuss each of these differences. Lodders (1995, 1996a,b) compared her results to the early eucritic composition experiments of Dickinson *et al.* (1990a,b,c) and to our early aubritic composition experiments that produced only Ca-poor oldhamite (Dickinson *et al.*, 1991). Our later aubritic experiments, which produced Ca-rich oldhamite, have been reported by Dickinson and McCoy (1996) and were discussed briefly by Lodders (1996b).

Lodders (1995, 1996a,b) used a bulk composition comprised of 200 mg silicate that was similar in composition to the silicate portion of enstatite chondrites mixed with ~200 mg of solid synthetic CaS. The silicate portion of the starting mix was prepared from major element oxides and carbonates (SiO_2, Al_2O_3, MgO, TiO_2, Na_2CO_3 and K_2CO_3) and REE-oxides. This starting composition was fused at 1500 °C in glassy C crucibles under N_2, producing ~20 wt% glass and ~80 wt% enstatite. X-ray diffraction analysis

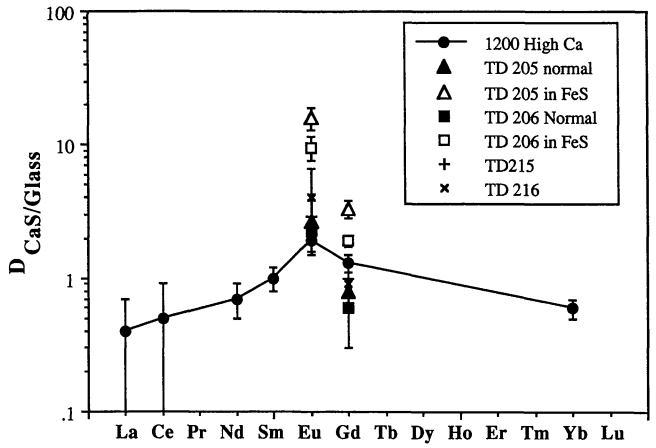

FIG. 4. Partition coefficients for 1200 °C experiments that produced Ca-rich oldhamite and 800 °C annealing experiments. The 800 °C experiments exhibit D_{Eu} uniformly elevated over the 1200 °C experiments and D_{Gd} that scatter around the 1200 °C D_{Gd} data. The most marked enrichments are in those oldhamites associated with FeS. Error bars are based on the standard deviation of the microprobe analyses of both the glass and sulfide as discussed in the text.

TABLE 9. Comparison of our data to literature data.

	J & B	Lodders		This Work	
T (°C)	1200	1300	1300	1200	1300
D		nor.	rev.		
La	0.4	0.41	–	0.4	0.3
Ce	–	–	–	0.5	0.6
Nd	–	–	–	0.8	1.2
Sm	–	0.34	1 23	1.0	1.8
Eu	–	1.14	2.16	1.9	1.2
Gd	12	0.34	1.24	1.3	2.2
Yb	–	1.44	–	0.7	2.9
Lu	24	1.04	–	–	–

References: J & B = Jones and Boynton (1983); Lodders = Lodders (1995, 1996a,b).
nor. = Rare earth elements initially in silicates; rev. = Rare earth elements initially in CaS.

showed that the synthetic CaS had the same structure as crystalline oldhamite. Lodders (1995, 1996a,b) did not add Fe to her initial mixture, which prevented crystallization of either FeS or Fe metal and, thus, precluded the independent calculation of fO_2 from phase compositions, as we have done. She did determine the ratio of fO_2/fS_2. Neither our starting composition nor that of Lodders (1995, 1996a,b) closely matches the compositions of aubrites (ours is enriched in Si and Al and Lodders, 1995, 1996a,b, contains no Fe; both are enriched in Ca and S), yet both sets of experiments prevent early crystallization of aluminous phases and crystallize enstatite and, thus, to some degree simulate aubrite crystallization.

The experiments of Lodders (1995, 1996a,b) were designed to equilibrate solid CaS with a mixture of enstatite and silicate melt at temperatures of 1200–1300 °C. Experiments of Lodders (1995, 1996a,b) were run as both normal experiments, where the silicate mixture was doped with REEs, and as reversal experiments, where the CaS was initially doped. It is important to note that Lodders (1995, 1996a,b) added solid CaS to her starting mixture and did not produce CaS by magmatic processes. This is in marked contrast to our experiments, where CaO and FeS_2 were added to the mixture, producing CaS during melting and crystallization. Thus, the experiments of Lodders (1995, 1996a,b) achieved partitioning by diffusion between the solid CaS and silicate melt, while our partition coefficients reflect incorporation of REEs during crystallization. Lodders (1996b) criticized our technique since it required sulfurization of CaO, which we agree is probably not the mechanism by which oldhamite formed in aubrites. However, if experiments using both methods reach equilibrium, there should be no difference in the measured partition coefficients. In these experiments, we are primarily interested in determining these silicate-oldhamite partition coefficients. Another set of experiments are in progress (McCoy *et al.*, 1997) to study the melting and differentiation of enstatite chondrites with applications to the formation of aubrites.

A difference between the experiments that we cannot fully evaluate is the influence of fO_2. Lodders (1995, 1996a,b) did not report fO_2 values for her experiments but did report ratios of fO_2/fS_2. Since no Fe was present in the starting material, an independent value for fO_2 could not be calculated from phase relations. Thus, no direct comparison can be made. However, given that partitioning seems to exhibit no dependence on O fugacity (discussed earlier) and that CaS is stable only at very reducing conditions, we believe that any differences in fO_2 between the two sets of experiments would have a negligible effect on REE partitioning.

The final difference between the two sets of experiments was run time. Despite initial problems with stability of the quartz tubes that enclosed our experiments, our final technique allowed typical run times of two days with no stability problems. In fact, we completed one run (TD-164) at 1200 °C for a period of seven days as a test of equilibrium. As we showed earlier, equilibrium was achieved in the two day runs and, in fact, probably within one day. In contrast, Lodders (1995, 1996a,b) experienced problems with stability of the quartz tubes enclosing her experiments. As such, her run times were significantly shorter, ranging from 16–26 h (Lodders et al., 1990; Lodders, 1996a,b). This is a particularly important difference, since the experiments of Lodders *et al.* (1990) and Lodders (1995, 1996a,b) required diffusion to attain equilibrium, and diffusion is a time-dependent process.

The partition coefficients for Lodders' (1995, 1996a,b) 1300 °C experiments are given in Table 9 and illustrated in Fig. 5. Lodders produced Ca-rich oldhamite (85–96% CaS) with REE partition coefficients generally <2 and inversely bowed REE patterns with positive Eu anomalies. An examination of her 1300 °C reversal data, however, suggests that equilibrium was not attained in the run times utilized. In experiments in which silicates were doped with Sm-Eu-Gd at 1300 °C, partition coefficients range from 0.3–1.2. In contrast, similar experiments with REE initially in the sulfide yield partition coefficients from 1.2–2.2, which is a factor of 2–4 higher than those in the silicate-doped experiments (Fig. 5). (Note that Lodders, 1995, 1996a,b, does not report errors on her partition coefficients.) This demonstrates that diffusive equilibrium between silicate melt and CaS was not completely achieved in the run times utilized. Since diffusion is a temperature-dependent process, one would expect equilibrium to be attained even slower at lower temperatures. Thus, silicate-doped experiments must be considered as lower limits to the true partition coefficients, while sulfide-doped experiments represent upper limits, thus leading to some uncertainty in determining the true partition coefficients in Lodders' (1995, 1996a,b) experiments. It seems clear, however, that the actual partition coefficients must lie between the values in the silicate- and sulfide-doped experiments. It is interesting to note that our partition coefficients for Sm, Eu and Gd in Ca-rich oldhamite lie between these values (Fig. 5). Lodders' (1995, 1996a,b) actual partition coefficients are poorly constrained for La, Yb or Lu, since no sulfide-doped experiments were reported for these elements. Thus, the only robust conclusions that one can draw from Lodders (1995, 1996a,b) appear to be that these patterns will all have positive Eu anomalies and that distribution coefficients are all <2.

We have examined four data sets (Jones and Boynton, 1983; Dickinson *et al.*, 1990a,b,c (eucritic), 1991 (aubritic); Lodders *et al.*, 1990; Lodders, 1995, 1996a,b) that use a variety of starting compositions and techniques, all of which yield partition coefficients <25, and most are <5. Thus, one must conclude that experimental partition coefficients, regardless of starting composition or technique, are roughly 1–2 orders of magnitude less than partition coefficients inferred from natural samples (Wheelock *et al.*, 1994).

DISCUSSION

There are three models for the origin of aubritic oldhamite: a simple igneous origin, a nebular origin and a complex igneous origin. Our new results bear directly on these potential origins. In this

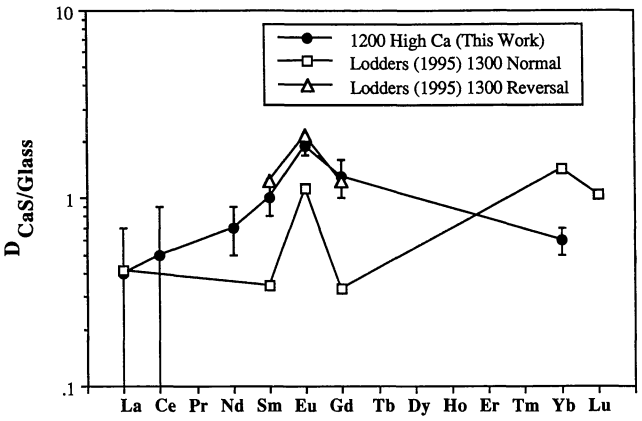

FIG. 5. Rare-earth-element partition coefficient patterns for 1200 °C Ca-rich oldhamite experiments and the 1300 °C equilibration experiments of Lodders (1995, 1996a). The experiments of Lodders (1995, 1996a) were run with REEs initially in silicates (normal) and in oldhamite (reversal) and equilibrium was not obtained. All three data sets suggest partition coefficients <5 and positive Eu anomalies. Error bars are based on the standard deviation of the microprobe analyses of both the glass and sulfide as discussed in the text.

section, we discuss our results, along with those of previous workers, to evaluate these models.

Simple Igneous Origin

A variety of processes could be combined under the category of simple igneous origins, including whole body melting and impact melting, but for the purpose of this discussion, they all include one important component: that oldhamite crystallizes at high temperature from the bulk melt and the REE pattern and abundances are determined solely by partitioning between crystallizing oldhamite and the bulk melt. Thus, the apparent partition coefficients inferred from comparison of natural oldhamite REE abundances and those in the bulk aubrites should be consistent with experimentally determined partition coefficients.

Our data is clearly inconsistent with such a model. Apparent distribution coefficients for natural oldhamite, calculated by dividing the REE abundance in oldhamite by the REE abundance in the bulk aubrite, range from 100 to 1000 (Wheelock *et al.*, 1994). Our data clearly show that experimental $D_{CaS/Glass}$ for a variety of REEs are typically <5. Thus, the REE abundances in natural oldhamite could not have been established by partitioning between a melt of bulk aubrite composition and oldhamite at temperatures of 1200–1300 °C. Given this fact, we now consider our data in light of the two other models.

Nebular Origin

At least four arguments have been given to suggest that aubritic oldhamite is, at least in part, a relict nebular phase that survived the extensive melting that altered the remainder of the meteorite. These are (1) the similarity in REE patterns of oldhamite in aubrites and unequilibrated enstatite chondrites, (2) the high melting temperature of oldhamite, (3) the occurrence of several oldhamite REE patterns in a single aubrite (Floss and Crozaz, 1993), and (4) S-isotopic anomalies in aubritic oldhamite (Thiemens *et al.*, 1994). Recent experimental work (Lodders, 1995, 1996a,b; Fogel *et al.*, 1996), including ours, can be used to address the first two of these issues and is discussed in greater detail below.

Similar Rare-earth-element Patterns in Aubrites and Unequilibrated Enstatite Chondrites–Floss *et al.* (1990), Floss and Crozaz (1993) and Crozaz and Lundberg (1995) have documented a variety of REE patterns in oldhamite in both aubrites and UECs. Floss *et al.* (1990) and Floss and Crozaz (1993) documented REE patterns in 109 oldhamite grains from four aubrites. These 109 grains exhibited 10 REE patterns (A–J, Fig. 5 of Floss and Crozaz, 1993). Crozaz and Lundberg (1995) documented seven REE patterns in six unequilibrated enstatite chondrites. An important conclusion of this body of work is that four of the ten oldhamite REE patterns observed in aubrites (patterns A, B, F and I; 70 of 109 grains) were similar to those in UECs and are difficult to explain by igneous fractionation. Since oldhamite in UECs is almost certainly of nebular origin (Crozaz and Lundberg, 1995), it seems likely that similar patterns in aubrites reflect the relict nebular origin of some aubritic oldhamite. Floss and Crozaz (1993) argued that the other six patterns were consistent with an igneous origin. Thus, oldhamite must have been near its melting point, thus leading to the combination of relict nebular and igneous oldhamites now found in aubrites. It is worth noting that both the igneous and nebular aubritic oldhamite grains of Floss and Crozaz (1993) exhibit REE abundances of ~100 × CI; they differ primarily in their REE patterns.

This appears to be, by far, the most compelling evidence for a relict nebular origin for some aubritic oldhamite. One of the prime criteria for selecting these four patterns as nebular is not only their similarity to REE patterns in UECs, but three of the patterns (A, F and I) exhibit Eu and, more importantly, Yb anomalies. The presence of these Eu and Yb anomalies are consistent with condensation calculations of Lodders and Fegley (1992), who showed that the Eu and Yb are more volatile than other REEs and, thus, would be depleted in early condensates and enriched in later condensates. Full condensation of REEs would result in the unfractionated pattern B. Thus, Eu and Yb anomalies can be explained through condensation.

However, the partition coefficients discussed above are not inconsistent with an igneous origin. Floss and Crozaz (1993) argued that no known mechanism existed to fractionate Yb from other REEs during magmatic or subsolidus processing and, thus, Yb anomalies require a nebular origin. Our experiments contained Yb but not Lu or Tm, so no information exists about a possible Yb anomaly. However, the experiments of Lodders (1995, 1996a,b) included both Yb and Lu and observed a marked Yb/Lu anomaly. Although no information is available about Tm partitioning, these data are not inconsistent with the presence of a positive Yb anomaly in the REE partition coefficients. Thus, while Yb anomalies are consistent with a nebular origin, they may not rule out an igneous origin.

High Melting Temperature of Oldhamite–Lodders *et al.* (1993) and Lodders (1995, 1996a,b) argued that aubritic oldhamite must be a relict phase, since the melting point of pure CaS is ~2450–2525 °C (Vogel and Heumann, 1941; Chase *et al.*, 1985) and temperatures on the aubrite parent body almost certainly never reached this temperature. In support of this view, Lodders (1995, 1996a) argued that temperatures of ~2500 °C would result in volatilization of Na and K, which are still present in aubrites. Even considering the solid solution of FeS, MnS and MgS in oldhamite at levels found in aubrites, Lodders *et al.* (1993) calculated a melting point of ~2350 °C for CaS.

Irregular grain boundaries with jagged edges and complex reentrant forms between enstatite grains in all aubrites suggest pyroxene co-crystallization, rather than formation as cumulates (Taylor *et al.*, 1993). This suggests crystallization from near-total melts of an enstatite-rich composition and a peak temperature near the melting point of pure enstatite (1560 °C). In addition, a growing experimental data base suggests that oldhamite probably cannot survive melting on the aubrite parent body, even at temperatures far below 2500 °C. Fogel *et al.* (1996) reported experiments on the melting of Indarch (EH4) and on Indarch mixed with synthetic CaS. These authors found in their 1400 °C run that no sulfides were present in the charge, with the glass having taken up all of the S. Lodders (1996b) has criticized these experiments because they are more reduced (19 wt% Si in Fe-metal) than would be expected on the aubrite parent body. Lodders (1996b) speculates that CaS will be less soluble under less reducing conditions. However, results similar to those of Fogel *et al.* (1996) were reported by Dickinson and Lofgren (1992) and McCoy *et al.* (1997) in their Indarch melting experiments . In these latter experiments, a Cr-metal O getter was used, which should produce appropriate reducing conditions. Large particles composed of immiscible Fe,Ni metal, FeS and (Fe, Mn, Mg, Ca)S and no unmelted sulfides were found in charges at temperatures as low as 1200 °C. The presence of Ca in one of the immiscible sulfide melts and lack of relict oldhamite grains strongly suggests that oldhamite melted completely. Both of these experiments were conducted at temperatures far below those inferred by Lodders *et al.* (1993) and probably below the peak temperature experienced by aubrites.

The likely reason for low-temperature melting of oldhamite is melting point depression of oldhamite in the presence of other sul-

fides and metal. Vogel and Heumann (1941) documented an FeS-CaS eutectic at 1120 °C for 80% FeS. This particular eutectic is highly relevant since oldhamite is commonly associated with troilite in UECs (Crozaz and Lundberg, 1995). The melting point depression of oldhamite in contact with other phases, particularly other sulfides and Fe,Ni metal, is unknown but may be well below the ~1600 °C peak temperature reached on the aubrite parent body. Thus, it appears likely that oldhamite, in the presence of metal or other sulfides, would melt readily on the aubrite parent body and this argues against a relict nebular origin for such oldhamites, as also concluded by Fogel *et al.* (1996) and McCoy *et al.* (1997).

Complex Igneous Origin

While our data are clearly inconsistent with a simple igneous origin as discussed above, it is worth considering them in the context of a more complex igneous origin. For our purposes, a complex igneous origin is one in which the REE abundances are not determined solely by partitioning during crystallization from a bulk melt but which may be effected by a variety of processes, including partial melting and melt removal, fractional crystallization and subsolidus annealing and exsolution. We note that previous authors who have advocated an igneous origin (*e.g.*, Fogel *et al.*, 1988; Taylor *et al.*, 1988; Keil, 1989; Wheelock *et al.*, 1994) have acknowledged that this origin must be complex. Given this complexity, high-temperature experimental REE oldhamite/silicate liquid partition coefficients may not match the apparent partition coefficients of 100–1000 for natural samples (Wheelock *et al.*, 1994). Here, we explore this origin in relation to our experiments.

Precursor Chondrite–Similarities in mineralogy and mineral and O-isotopic compositions support the view that aubrites formed from a precursor similar, but not identical, to enstatite chondrites (Keil, 1968; Watters and Prinz, 1979; Clayton *et al.*, 1984; Brett and Keil, 1986; Keil, 1989). An enstatite chondrite precursor would likely contain oldhamite in a variety of petrologic settings, including intimately associated with troilite (FeS), niningerite ((Mg,Fe)S) and metal (Crozaz and Lundberg, 1995). We would also expect the chondritic precursor to have essentially flat REE abundances, although EL chondrites exhibit a slightly fractionated bulk La/Sm ratio (Kallemeyn and Wasson, 1986).

Melting and Differentiation–As the aubrite parent body was heated to the peak temperature (1500–1600 °C, as discussed earlier), partial melting, melt migration and fractionation likely occurred. Partial melting of a chondritic precursor at the Fe,Ni-FeS cotectic (~85% FeS, 15% Fe,Ni) occurs at ~980 °C, and the first silicate (basaltic) melting occurs at ~1050 °C (Kullerud, 1963; Taylor *et al.*, 1993). It seems likely that these melts were removed efficiently, but not completely, because of the marked depletion of aubrites in plagioclase, metal and troilite compared to enstatite chondrites (Keil, 1968; Watters and Prinz, 1979). These phases may have been removed in partial melts, perhaps by explosive volcanism (Wilson and Keil, 1991). However, we cannot rule out that these phases were partially removed during later fractional crystallization of the aubrite parent body (Watters and Prinz, 1979). Removal of the basaltic partial melt, which contains Eu-rich plagioclase, will result in depletion of the residue in bulk REE and probably formation of a negative Eu anomaly. We would note that in the Wilson and Keil (1991) model, these melts are not just segregated to another part of the body but rather wholly removed from the aubrite parent body. Thus, continued heating and total melting of the aubrite parent body cannot reassimilate these melts and, thus, cannot return the bulk aubrite system to chondritic REE abundances.

At the peak temperature reached by the aubrite parent body (1500–1600 °C), melting would have been extensive. The bulk silicates would be completely molten, and earlier removal of silicate partial melts would probably result in a fractionated REE pattern relative to the chondritic precursor. In addition, experimental evidence suggests that most, if not all, oldhamite, other sulfides and metal would have melted. This oldhamite might exist either as part of an immiscible sulfide melt within the silicate melt, as CaS dissolved in the silicate melt or both (Fogel *et al.*, 1996; McCoy *et al.*, 1997). Note that we are not arguing for formation of oldhamite *via* sulfurization of CaO but rather melting of preexisting oldhamite with later crystallization. Similar processes could have occurred in the simple igneous model, as we have defined it. The distinction between simple and complex igneous processes depends on whether oldhamite is the first crystallizing phase from this bulk melt and its REE abundances and patterns are unchanged during cooling, or whether more complex processes act to determine the REE abundances of the melt, and thus the oldhamite, during crystallization and cooling.

Fractional Crystallization–Previous workers advocating an igneous origin for aubrites have argued that fractional crystallization of the parent magma(s) played a significant role in producing the range of igneous lithologies observed (Fogel *et al.*, 1988; Taylor *et al.*, 1988), and it may have significantly increased the REE content of the melt from which oldhamite crystallized. Aubrites typically contain 80–90% enstatite and 1–10% forsterite (Watters and Prinz, 1979). Since enstatite and forsterite are essentially devoid of REE (Wheelock *et al.*, 1994), crystallization of these phases would enrich the melt in REE. Crystallization of 90% silicates would result in an increase in REE abundances by a factor of 10, while 99% silicate crystallization would result in a factor of 100 increase. Significant silicate crystallization would also enrich the melt in Ca, thus allowing crystallization of CaS and possibly plagioclase, which would further fractionate the REEs in the melt. In addition, extensive silicate crystallization isolates remaining melt pockets, thus allowing independent chemical evolutions and production of a variety of REE patterns.

Evidence for silicate crystallization prior to oldhamite crystallization comes from both petrologic and experimental studies. Wheelock *et al.* (1994) illustrate oldhamite partially enclosing forsterite in the Norton County oldhamite-rich lithology, which suggests crystallization of forsterite while oldhamite was still molten. Indarch partial melting experiments at 1400–1425 °C (Dickinson and Lofgren, 1992; Fogel *et al.*, 1996) contain no relict oldhamite but significant enstatite. We estimate that the 1425 °C experiment of Dickinson and Lofgren (1992) contains ~40% enstatite. Thus, significant silicate crystallization likely played a role in increasing the REE content of the melt from which oldhamite crystallized.

The diversity of REE patterns observed in aubrites might also reflect, at least in part, the composition of the crystallizing oldhamite. We have shown that the REE partition coefficients are dependent on oldhamite composition and, thus, a single magma might produce oldhamite of different composition and different REE patterns. While aubritic oldhamite is typically very calcic (Watters and Prinz, 1979; Wheelock *et al.*, 1994), several papers on the REE patterns of aubritic oldhamite (Floss *et al.*, 1990; Floss and Crozaz, 1993) did not report the major element composition of the oldhamite. In addition, the presence of exsolved Fe-Mg-Mn-rich phases within some aubritic oldhamite (*e.g.*, Wheelock *et al.*, 1994) suggests that at least some aubritic oldhamite was less calcic at magmatic temperatures.

Annealing and Exsolution–Annealing and exsolution may have also influenced REE patterns in natural oldhamite. It seems clear that aubrites experienced a period of slow cooling after crystallization, as demonstrated by metallographic cooling rates of 1–100 °C/Ma (Okada *et al.*, 1988). Our 800 °C annealing experiments produced partition coefficients for Eu a factor of eight higher than in the magmatic partitioning experiments.

Aubrites also contain a variety of phases that exsolved from magmatic sulfide. A more important observation is that our experiments represent the partitioning of REE into oldhamite quenched from 1200 °C. Wheelock *et al.* (1994) observed centimeter-sized oldhamite grains with ~10% exsolved ferromagnesian alabandite ((Mn,Mg,Fe)S). The oldhamite and exsolved alabandite have significantly different REE patterns (Wheelock *et al.*, 1994). It is possible that the high-temperature oldhamite prior to exsolution of alabandite had a different major and REE composition from that observed in the current oldhamite. It is this preexsolution oldhamite with which our experiments should be compared. Studies of natural oldhamite in aubrites should examine any exsolution phases as well. Rare-earth-element patterns, thus, appear to be affected by solid-solid partition coefficients between the host oldhamite and the exsolved phases. This process as well as the associated solid-solid partition coefficients have not been experimentally studied.

CONCLUSIONS

Our experiments produced crystalline oldhamite from melts at temperatures of 1200–1300 °C, which is far below the melting point of pure oldhamite (~2450–2525 °C). Partitioning of REEs between oldhamite and silicate melt appear to be strongly dependent on oldhamite composition and temperature (both magmatic and subsolidus). No dependence was noted with O fugacity or REE content. Oldhamite/silicate liquid REE partition coefficients are generally around unity and the REE partition coefficient pattern exhibits a positive Eu anomaly as found by others. Annealing experiments produced D_{Eu} up to 16.1, also with a positive Eu anomaly. Experimental partition coefficients are clearly inconsistent with a simple igneous model, in which oldhamite is the first crystallizing phase and REE abundances are determined solely by high-temperature partitioning between oldhamite and the bulk liquid. Our experimental partition coefficients are consistent with a nebular model, in which oldhamite in aubrites is a nebular relict that survived melting. However, experimental evidence that suggests melting of oldhamite at temperatures lower than that reached on the aubrite parent body are clearly inconsistent with the nebular model. Our experiments are also consistent with a complex igneous history. Oldhamite REE patterns may reflect a complex process of partial melting, melt removal, fractional crystallization and subsolidus annealing and exsolution. These mechanisms (primarily fractional crystallization and subsolidus annealing) can produce a wide range of REE patterns in aubritic oldhamite, as well as elevated (100–1000 × CI) REE abundances observed in aubritic oldhamite.

Acknowledgments–We would like to thank A. Jurewicz and S. Jurewicz for help in running experiments. R. Martinez and M. Zolensky provided results of XRD analysis of the separated oldhamite. P. Bernhard prepared polished thin sections. V. Yang provided assistance in microprobe analyses. Useful discussion and comments on this manuscript were provided by G. E. Lofgren, J. Nuth, G. A. McKay, A. Jurewicz, S. Jurewicz, M. M. Wheelock, I. Casanova and V. Hillgren. Comments by K. Lodders, D. M. Shaw and an anonymous reviewer clarified the manuscript, although they may not endorse the conclusions. This work was supported, in part, by National Research Council Postdoctoral Fellowships to both authors and NASA grant NCC-5-83 (TLD).

Editorial handling: D. M. Shaw

REFERENCES

BRETT R. AND KEIL K. (1986) Enstatite chondrites and enstatite achondrites (aubrites) were not derived from the same parent body. *Earth Planet. Sci. Lett.* **81,** 1–6.

CASANOVA I. (1990) Geochemistry of metal segregation in aubrites and the origin of their metallic phases. Ph.D. dissertation, University of New Mexico. 97 pp.

CHASE M. W., DAVIES C. A., DOWNING J. R., FRURIP D. J., MCDONALD R. A. AND SYVERUD A. N. (1985) JANAF thermochemical tables. *J. Phys. Chem. Ref. Data* **14, Suppl. 1.**

CLAYTON R. N., MAYEDA T. K. AND RUBIN A. E. (1984) Oxygen isotopic compositions of enstatite chondrites and aubrites. *Proc. Lunar Planet. Sci. Conf.* **15th,** C245–C249.

CROZAZ G. AND LUNDBERG L. L. (1995) The origin of oldhamite in unequilibrated enstatite chondrites. *Geochim. Cosmochim. Acta* **59,** 3817–3831.

DICKINSON T. L. AND LOFGREN G. E. (1992) Melting relations for Indarch (EH4) under reducing conditions (abstract). *Lunar Planet. Sci.* **23,** 307–308.

DICKINSON T. L. AND MCCOY T. J. (1996) Experimental REE partitioning in oldhamite: Applications for the igneous origin of aubritic oldhamite (abstract). *Lunar Planet. Sci.* **27,** 309–310.

DICKINSON T. L., LOFGREN G. E. AND MCKAY G. A. (1990a) REE partitioning between silicate liquid and immiscible sulfide liquid: The origin of the negative Eu anomaly in aubrite sulfides (abstract). *Lunar Planet. Sci.* **21,** 284–285.

DICKINSON T. L., LOFGREN G. E. AND MCKAY G. A. (1990b) Sulfide fractionation and the origin of the negative Eu anomaly in aubrites (abstract). *Meteoritics* **25,** 358.

DICKINSON T. L., LOFGREN G. E. AND MCKAY G. A. (1990c) REE partitioning between silicate liquid and immiscible sulfide liquid: The origin of aubritic sulfides (abstract). *EOS Trans. AGU* **71,** 1434.

DICKINSON T. L., LOFGREN G. E. AND MCKAY G. A. (1991) On the magmatic origin of oldhamite in aubrites (abstract). *Lunar Planet. Sci.* **22,** 319–320.

DRAKE M. J. AND WEILL D. F. (1972) New rare earth element standards for electron microprobe analysis. *Chem. Geol.* **10,** 179–181.

FLOSS C. AND CROZAZ G. (1993) Heterogeneous REE patterns in oldhamite from the aubrites: Their nature and origin. *Geochim. Cosmochim. Acta* **57,** 4039–4057.

FLOSS C., STRAIT M. M. AND CROZAZ G. (1990) Rare earth elements and the petrogenesis of aubrites. *Geochim. Cosmochim. Acta* **57,** 4039–4057.

FOGEL R. A., HESS P. C. AND RUTHERFORD M. J. (1988) The enstatite chondrite-achondrite link (abstract). *Lunar Planet. Sci.* **19,** 342–343.

FOGEL R. A., HESS P. C. AND RUTHERFORD M. J. (1989) Intensive parameters of the enstatite chondrite metamorphism. *Geochim. Cosmochim. Acta* **53,** 2735–2746.

FOGEL R. A., WEISBERG M. K AND PRINZ M. (1996) The solubility of CaS in aubrite silicate melts (abstract). *Lunar Planet. Sci.* **27,** 371–372.

HILLGREN V. J., DRAKE M. J. AND RUBIE D. C. (1996) High pressure and high temperature metal-silicate partitioning of siderophile elements: The importance of silicate liquid composition. *Geochim. Cosmochim. Acta* **60,** 2257–2263.

JONES J. H. AND BOYNTON W. V. (1983) Experimental geochemistry in very reducing systems: Extreme REE fractionation by immiscible sulfide liquids (abstract). *Lunar Planet. Sci.* **14,** 353–354.

KALLEMEYN G. W. AND WASSON J. T. (1986) Compositions of enstatite (EH3, EH4,5 and EL6) chondrites: Implications regarding their formation. *Geochim. Cosmochim. Acta* **50,** 2153–2164.

KEIL K. (1968) Mineralogical and chemical relationships among enstatite chondrites. *J. Geophys. Res.* **73,** 6945–6976.

KEIL K. (1989) Enstatite meteorites and their parent bodies. *Meteoritics* **24,** 195–208.

KULLERUD G. (1963) The Fe-Ni-S system. *Ann. Rep. Geophys. Res.* **67,** 4055–4061.

KURAT G., ZINNER E. AND BRÄNDSTATTER F. (1992) An ion microprobe study of an unique oldhamite-pyroxenite fragment from the Bustee aubrite (abstract). *Meteoritics* **27,** 246–247.

LARIMER J. W. AND GANAPATHY R. (1987) The trace element chemistry of CaS in enstatite chondrites and some implications regarding its origin. *Earth Planet. Sci. Lett.* **84,** 123–124.

LODDERS K. (1995) Experimental partitioning of rare earth elements between sulfides (FeS, CaS) and silicate melt and applications to enstatite achondrites (abstract). *NIPR Symp. Antarct. Meteor.* **20,** 140–143.

LODDERS K. (1996a) Oldhamite in enstatite achondrites (aubrites). *Proc. NIPR Symp. Antarct. Meteor.* **9th,** 127–142.

LODDERS K. (1996b) An experimental and theoretical study of rare-earth-element partitioning between sulfides (FeS,CaS) and silicate and applications to enstatite achondrites. *Meteorit. Planet. Sci.* **31,** 749–766.

LODDERS K. AND FEGLEY B. (1992) Lanthanide and actinide condensation into oldhamite under reducing conditions (abstract). *Lunar Planet. Sci.* **23,** 797–798.

LODDERS K. AND PALME H. (1989) Europium anomaly produced by sulfide separation and implications for the formation of enstatite achondrites (aubrites) (abstract). *Meteoritics* **24,** 293–294.

LODDERS K. AND PALME H. (1990) Fractionation of REE during aubrite formation: The influence of FeS and CaS (abstract). *Lunar Planet. Sci.* **21,** 710–711.

LODDERS K., PALME H. AND DRAKE M. J. (1990) The origin of oldhamite in enstatite achondrites (aubrites) (abstract). *EOS Trans. AGU* **71,** 1434.

LODDERS K., PALME H. AND WLOTZKA F. (1993) Trace elements in mineral separates of the Peña Blanca Spring aubrite: Implications for the evolution of the aubrite parent body. *Meteoritics* **28,** 538–551.

MCCOY T. J., DICKINSON T. L. AND LOFGREN G. E. (1997) Partial melting of Indarch (EH4) chondrite from 1000–1425 °C: New insights into igneous processes in enstatite meteorites (abstract). *Lunar Planet. Sci.* **28,** 903–904.

OKADA A., KEIL K., TAYLOR G. J. AND NEWSOM H. E. (1988) Igneous history of the aubrite parent asteroid: Evidence from the Norton County enstatite achondrite. *Meteoritics* **23,** 59–74.

RICHTER G. R., WOLF R. AND ANDERS E. (1979) Aubrites: Are they direct nebular condensates? (abstract) *Lunar Planet. Sci.* **10,** 1028–1030.

ROBIE R. A., HEMINGWAY B. S. AND FISHER J. R. (1978) *Thermodynamic Properties of Minerals and Related Substances at 298. 15K and 1 Bar Pressure and at Higher Temperatures.* Geological Survey Bulletin **1452,** United States Printing Office, Washington D.C. 456 pp.

SAKAO H. AND ELLIOT J. F. (1975) Thermodynamics of dilute bcc Fe-Si alloys. *Met. Trans. A* **6A,** 1849–1851.

SEARS D. W. G. (1980) Formation of E-chondrites and aubrites–A thermodynamic model. *Icarus* **43,** 184–202.

SHIMAOKA T. K., SHINOTSUKA K., EBIHARA M. AND PRINZ M. (1995) Whole rock compositions of aubritic meteorites: Implications for their origin (abstract). *Lunar Planet. Sci.* **26,** 1291–1292.

TAYLOR G. J., KEIL K., NEWSOM H. AND OKADA A. (1988) Magmatism and impact on the aubrite parent body: Evidence from the Norton County enstatite achondrite (abstract). *Lunar Planet. Sci.* **19,** 1185–1186.

TAYLOR G. J., KEIL K., MCCOY T., HAACK H. AND SCOTT E. R. D. (1993) Asteroid differentiation: Pyroclastic volcanism to magma ocean. *Meteoritics* **28,** 34–52.

THIEMENS M. H., BREARLEY A., JACKSON T. AND BOBIAS G. (1994) Detection of a ^{35}S excess in an oldhamite separate from Norton County (abstract). *Meteoritics* **29,** 540–541.

VOGEL R. AND HEUMANN T. (1941) Das System Eisen-Eisensulfid-Kalziumsulfid. *Archiv Eisenhüttenw.* **15,** 195–199.

WASSON J. T. AND WAI C. M. (1970) Composition of the metal, schreibersite and perryite of enstatite achondrites and the origin of enstatite chondrites and achondrites. *Geochim. Cosmochim. Acta* **34,** 169–184.

WATTERS T. R. AND PRINZ M. (1979) Aubrites: Their origin and relationship to chondrites. *Proc. Lunar Planet. Sci. Conf.* **10th,** 1073–1093.

WHEELOCK M. M., KEIL K., FLOSS C., TAYLOR G. J. AND CROZAZ G. (1994) REE geochemistry of oldhamite-dominated clasts from the Norton County aubrite: Igneous origin of oldhamite. *Geochim. Cosmochim. Acta* **58,** 449–458.

WILSON L. AND KEIL K. (1991) Consequences of explosive eruptions on small Solar System bodies: The case of the missing basalt on the aubrite parent body. *Earth Planet. Sci. Lett.* **104,** 505–512.

Appendix appears on the following pages

APPENDIX 1. Average glass, oldhamite and metal compositions (wt%) in our experiments.

Sample Number	Temp °C	Time Days	REE	REE Conc. wt%	Buffer	Mg	Al	Si	S	Ca	Fe	La	Ce	Nd	Sm	Eu	Gd	Yb
Glass Compositions																		
TLD 153	1300	2	Eu, Gd	1	–	9.10	4.82	26.41	6.77	9.71	0.32	–	–	–	–	1.42	1.06	–
TLD 158	1300	2	Sm, Nd, Yb	1	–	10.54	5.06	28.23	7.50	8.83	0.29	–	–	1.01	1.56	–	–	0.77
TLD 171	1300	2	La, Ce	1	–	9.72	5.45	25.18	6.99	9.33	0.23	1.70	1.35	–	–	–	–	–
TLD 157	1200	2	Sm, Nd, Yb	1	–	5.81	7.82	31.06	4.02	8.23	0.25	–	–	0.64	1.32	–	–	0.81
TLD 155	1200	2	La, Ce	1	–	6.72	7.71	28.53	5.41	8.07	0.26	1.95	2.18	–	–	–	–	–
TLD 154	1200	2	Eu, Gd	1	–	5.53	7.63	29.40	3.60	8.02	0.20	–	–	–	–	1.55	1.42	–
TLD 161	1200	2	Eu, Gd	2	–	5.68	6.94	27.40	4.12	7.94	0.18	–	–	–	–	2.85	2.56	–
TLD 162	1200	2	Eu, Gd	0.5	–	5.99	7.63	29.42	4.04	7.80	0.17	–	–	–	–	0.78	0.60	–
TLD 164	1200	7	Eu, Gd	1	0.25 MgO	5.60	7.49	26.98	4.55	7.85	0.12	–	–	–	–	1.79	1.26	–
TLD 173	1200	2	Eu, Gd	1	–	4.60	7.10	27.70	3.20	9.60	0.13	–	–	–	–	0.98	1.30	–
TLD 174	1200	2	Eu, Gd	1	–	5.01	6.83	28.93	3.08	9.56	0.17	–	–	–	–	0.97	1.30	–
TLD 176	1200	2	La, Ce	0.25	–	5.71	7.46	29.14	3.84	8.55	0.22	0.71	0.28	–	–	–	–	–
TLD 177	1200	2	La, Ce	4	–	5.97	6.00	26.30	4.54	8.70	0.16	4.45	5.69	–	–	–	–	–
TLD 178	1200	2	Eu, Gd	0.25	–	5.47	7.85	28.95	4.07	8.74	0.14	–	–	–	–	0.66	0.14	–
TLD 179	1200	2	Eu, Gd	4	–	6.30	7.40	25.40	4.10	8.70	0.18	–	–	–	–	3.56	4.01	–
TLD 180	1200	2	Sm, Nd, Yb	0.25	–	5.10	7.53	28.92	3.67	9.20	0.10	–	–	0.33	0.31	–	–	0.32
TLD 183	1200	2	Eu, Gd	1	–	6.30	7.53	27.47	3.78	9.13	0.20	–	–	–	–	1.49	1.34	–
TLD 185	1200	2	Sm, Nd, Yb	4	–	5.90	5.74	26.15	4.37	7.64	0.16	–	–	4.31	3.34	–	–	3.72
TLD 196	1200	2	Eu, Gd	1	–	5.06	6.67	28.66	3.07	10.39	0.20	–	–	–	–	1.10	1.60	–
TLD 197	1200	2	Eu, Gd	1	–	5.30	6.97	28.36	3.20	10.77	0.15	–	–	–	–	1.15	1.09	–
TLD 198	1200	2	Eu, Gd	1	–	5.80	7.10	28.06	3.40	10.20	0.91	–	–	–	–	1.15	1.37	–
TLD 199	1200	2	Eu, Gd	1	–	5.03	6.78	29.05	3.20	10.20	0.09	–	–	–	–	1.21	1.32	–
TLD 200	1200	2	Eu, Gd	1	–	4.93	6.79	29.14	3.10	10.40	0.22	–	–	–	–	1.17	1.63	–
TLD 205	1200/800	2/9	Eu, Gd	1	–	3.78	6.37	28.96	3.14	11.60	0.41	–	–	–	–	1.10	1.49	–
TLD 206	1200/800	2/9	Eu, Gd	1	–	3.60	6.50	29.30	2.80	11.60	0.19	–	–	–	–	1.19	1.53	–
TLD 208	1200	2	Sm, Nd, Yb	1	–	5.29	5.42	28.40	3.07	11.42	0.15	–	–	1.06	1.06	–	–	1.63
TLD 209	1200	2	Sm, Nd, Yb	1	–	7.28	4.69	28.83	2.57	9.97	0.34	–	–	0.76	0.78	–	–	1.26
TLD 211	1200	2	La, Ce	1	–	5.30	5.72	28.78	3.03	11.70	0.16	1.03	1.22	–	–	–	–	–
TLD 212	1200	2	La, Ce	1	–	5.27	5.84	28.87	2.97	11.74	0.15	0.98	1.11	–	–	–	–	–
TLD 215	1200/800	2/9	Eu, Gd	1	–	4.17	6.78	28.07	2.54	10.85	0.20	–	–	–	–	1.04	1.64	–
TLD 216	1200/800	2/9	Eu, Gd	1	–	4.06	7.43	27.67	2.99	11.22	0.16	–	–	–	–	1.41	2.39	–
TLD 218	1200	2	Sm, Nd, Yb	1	–	5.20	6.90	27.90	3.50	10.00	0.06	–	–	1.20	1.20	–	–	1.00
TLD 219	1200	2	Sm, Nd, Yb	1	–	5.40	7.10	27.50	3.40	10.00	0.09	–	–	1.30	1.20	–	–	1.00
TLD 225	1200	2	Eu, Gd	1	Cr	6.10	6.80	25.40	2.80	11.60	0.13	–	–	–	–	1.90	2.30	–
TLD 228	1200	2	Eu, Gd	1	Mg	7.10	8.50	25.70	3.10	10.20	0.16	–	–	–	–	1.00	1.35	–
TLD 229	1200	2	Eu, Gd	1	C	6.30	6.20	26.90	2.20	12.60	0.16	–	–	–	–	0.69	1.30	–
TLD 232	1200	2	Eu, Gd	1	V	7.00	7.90	23.30	2.20	11.46	0.23	–	–	–	–	2.30	2.70	–
CaS Compositions																		
TLD 153	1300	2	Eu, Gd	1	–	9.57	0.02	0.11	44.96	34.15	6.42	–	–	–	–	1.66	2.38	–
TLD 158	1300	2	Sm, Nd, Yb	1	–	10.23	0.00	0.14	44.14	35.67	2.43	–	–	1.25	2.84	–	–	2.20
TLD 171	1300	2	La, Ce	1	–	6.78	0.15	0.34	44.24	42.87	1.05	0.55	0.82	–	–	–	–	–
TLD 157	1200	2	Sm, Nd, Yb	1	–	8.41	0.00	0.14	42.78	32.40	7.62	–	–	2.11	4.59	–	–	3.53
TLD 155	1200	2	La, Ce	1	–	9.39	0.17	0.47	43.95	37.45	3.60	0.91	2.12	–	–	–	–	–
TLD 154	1200	2	Eu, Gd	1	–	5.25	0.10	0.42	41.01	39.62	2.56	–	–	–	–	2.67	4.95	–
TLD 161	1200	2	Eu, Gd	2	–	4.70	0.19	0.56	40.83	38.22	1.73	–	–	–	–	5.09	7.10	–
TLD 162	1200	2	Eu, Gd	0.5	–	7.18	0.16	0.18	43.24	40.34	2.49	–	–	–	1.03	2.46	–	–

APPENDIX 1. *Continued.*

Sample Number	Temp °C	Time Days	REE	REE Conc. wt%	Buffer	Mg	Al	Si	S	Ca	Fe	La	Ce	Nd	Sm	Eu	Gd	Yb
CaS Compositions *(continued)*																		
TLD 164	1200	7	Eu, Gd	1	0.25 MgO	6.33	0.10	0.27	44.48	39.96	1.12	–	–	–	–	2.93	4.61	–
TLD 173	1200	2	Eu, Gd	1	–	2.90	0.00	0.20	40.60	42.40	2.80	–	–	–	–	1.80	2.60	–
TLD 174	1200	2	Eu, Gd	1	–	2.93	0.04	0.17	41.76	43.93	2.99	–	–	–	–	1.90	2.65	–
TLD 176	1200	2	La, Ce	0.25	–	6.17	0.05	0.20	45.01	41.18	4.93	0.41	0.32	–	–	–	–	–
TLD 177	1200	2	La, Ce	4	–	3.14	0.09	0.42	42.10	45.05	1.79	1.41	3.39	–	–	–	–	–
TLD 178	1200	2	Eu, Gd	0.25	–	6.79	0.22	0.29	44.59	40.18	4.42	–	–	–	–	0.86	0.63	–
TLD 179	1200	2	Eu, Gd	4	–	3.19	0.12	0.38	39.36	37.62	2.22	–	–	–	–	7.49	6.65	–
TLD 180	1200	2	Sm, Nd, Yb	0.25	–	3.85	0.01	0.35	42.96	42.81	2.40	–	–	0.60	0.82	–	–	1.12
TLD 183	1200	2	Eu, Gd	1	–	3.76	0.10	0.10	42.59	41.02	3.61	–	–	–	–	2.95	3.04	–
TLD 185	1200	2	Sm, Nd, Yb	4	–	3.76	0.00	0.26	37.19	31.42	2.41	–	–	5.93	6.61	–	–	9.69
TLD 196	1200	2	Eu, Gd	1	–	2.10	0.13	0.47	40.90	43.30	4.40	–	–	–	–	2.20	2.04	–
TLD 197	1200	2	Eu, Gd	1	–	2.70	0.45	1.76	38.68	42.48	2.30	–	–	–	–	2.20	1.45	–
TLD 198	1200	2	Eu, Gd	1	–	2.10	0.43	1.48	39.22	42.38	5.28	–	–	–	–	2.18	1.70	–
TLD 199	1200	2	Eu, Gd	1	–	2.50	0.92	1.59	37.69	42.47	2.28	–	–	–	–	2.30	1.88	–
TLD 200	1200	2	Eu, Gd	1	–	2.10	0.03	0.22	43.18	45.03	2.25	–	–	–	–	2.34	2.11	–
TLD 205	1200/800	2/9	Eu, Gd	1	–	0.29	0.15	0.52	41.60	47.80	1.90	–	–	–	–	3.02	1.16	–
TLD 205	1200/800	2/9	Eu, Gd	1	–	0.21	0.06	0.04	35.80	35.70	1.85	–	–	–	–	17.82	4.97	–
TLD 206	1200/800	2/9	Eu, Gd	1	–	0.31	0.11	0.38	42.00	48.60	1.68	–	–	–	–	2.78	0.90	–
TLD 206	1200/800	2/9	Eu, Gd	1	–	0.20	0.05	0.21	38.10	41.40	2.10	–	–	–	–	11.50	2.90	–
TLD 208	1200	2	Sm, Nd, Yb	1	–	1.80	0.04	0.50	40.30	44.20	3.20	–	–	0.76	1.06	–	–	1.02
TLD 209	1200	2	Sm, Nd, Yb	1	–	1.60	0.12	0.61	37.90	42.80	3.94	–	–	0.77	1.10	–	–	1.09
TLD 211	1200	2	La, Ce	1	–	1.81	0.06	0.28	40.23	46.13	3.45	0.32	0.56	–	–	–	–	–
TLD 212	1200	2	La, Ce	1	–	1.73	0.11	0.30	39.54	44.15	5.04	0.37	0.65	–	–	–	–	–
TLD 215	1200/800	2/9	Eu, Gd	1	–	0.46	0.04	0.20	39.71	46.01	1.54	–	–	–	–	3.05	1.70	–
TLD 216	1200/800	2/9	Eu, Gd	1	–	0.31	0.04	0.19	40.29	46.15	1.68	–	–	–	–	5.79	1.87	–
TLD 218	1200	2	Sm, Nd, Yb	1	–	2.50	0.13	1.30	37.00	42.10	1.90	–	–	1.20	1.60	–	–	3.10
TLD 219	1200	2	Sm, Nd, Yb	1	–	2.70	0.26	1.50	36.90	41.40	0.47	–	–	1.20	1.60	–	–	3.20
TLD 225	1200	2	Eu, Gd	1	Cr	1.60	0.19	0.90	36.40	41.60	2.10	–	–	–	–	3.10	1.30	–
TLD 228	1200	2	Eu, Gd	1	Mg	3.00	1.20	4.10	38.10	41.60	0.49	–	–	–	–	2.00	1.50	–
TLD 229	1200	2	Eu, Gd	1	C	1.90	0.00	0.03	41.40	45.00	2.70	–	–	–	–	1.90	1.30	–
TLD 232	1200	2	Eu, Gd	1	V	2.90	1.00	3.00	35.00	37.80	4.80	–	–	–	–	4.30	1.90	–
Fe Compositions																		
TLD 153	1300	2	Eu, Gd	1	–	0.05	0.01	5.37	0.58	0.31	92.00	–	–	–	–	0.04	0.02	–
TLD 158	1300	2	Sm, Nd, Yb	1	–	0.19	0.21	13.08	0.09	0.25	86.71	–	–	0.04	0.03	–	–	0.02
TLD 171	1300	2	La, Ce	1	–	0.01	0.02	12.40	0.06	0.09	88.18	0.04	0.05	–		–	–	–
TLD 157	1200	2	Sm, Nd, Yb	1	–	0.04	0.08	5.64	0.11	0.09	94.90	–	–	0.04	0.01	–	–	0.04
TLD 155	1200	2	La, Ce	1	–	0.00	0.01	10.67	0.12	0.06	94.45	0.09	0.02	–	–	–	–	–
TLD 154	1200	2	Eu, Gd	1	–	0.00	0.01	6.46	0.04	0.21	92.10	–	–	–	–	0.02	0.03	–
TLD 161	1200	2	Eu, Gd	2	–	0.00	0.02	10.71	0.10	0.09	90.72	–	–	–	–	0.04	0.02	–
TLD 162	1200	2	Eu, Gd	0.5	–	0.01	0.06	9.47	0.26	0.17	91.89	–	–	–	–	0.01	0.02	–
TLD 164	1200	7	Eu, Gd	1	0.25 MgO	0.00	0.04	14.11	0.03	0.07	86.81	–	–	–	–	0.02	0.01	–
TLD 173	1200	2	Eu, Gd	1	–	0.00	0.06	2.20	0.64	0.09	93.30	–	–	–	–	0.00	0.00	–
TLD 174	1200	2	Eu, Gd	1	–	0.02	0.03	2.63	0.69	0.16	92.69	–	–	–	–	0.03	0.01	–
TLD 176	1200	2	La, Ce	0.25	–	0.17	0.14	5.03	0.29	0.28	93.10	0.03	0.02	–	–	–	–	–
TLD 177	1200	2	La, Ce	4	–	0.67	0.04	6.94	0.26	0.37	91.57	0.09	0.20	–	–	–	–	–

APPENDIX 1. *Continued.*

Sample Number	Temp °C	Time Days	REE	REE Conc. wt%	Buffer	Mg	Al	Si	S	Ca	Fe	La	Ce	Nd	Sm	Eu	Gd	Yb
Fe Compositions *(continued)*																		
TLD 178	1200	2	Eu, Gd	0.25	–	0.01	0.04	5.14	0.35	0.16	95.09	–	–	–	–	0.01	0.00	–
TLD 179	1200	2	Eu, Gd	4	–	0.02	0.06	4.60	0.16	0.17	94.72	–	–	–	–	0.06	0.03	–
TLD 180	1200	2	Sm, Nd, Yb	0.25	–	0.00	0.01	6.50	0.02	0.04	95.91	–	–	0.01	0.00	–	–	0.01
TLD 180	1200	2	Sm, Nd, Yb	0.25	–	0.00	0.00	20.22	0.00	0.02	81.40	–	–	0.02	0.02	–	–	0.02
TLD 180	1200	2	Sm, Nd, Yb	0.25	–	0.02	0.00	32.60	0.02	0.00	69.40	–	–	0.04	0.13	–	–	0.00
TLD 183	1200	2	Eu, Gd	1	–	0.00	0.01	2.86	0.80	0.06	96.95	–	–	–	–	0.30	0.00	–
TLD 185	1200	2	Sm, Nd, Yb	4	–	0.00	0.00	7.95	0.03	0.14	93.72	–	–	–	–	0.05	0.07	–
TLD 196	1200	2	Eu, Gd	1	–	0.00	0.02	2.40	0.70	0.02	92.80	–	–	–	–	0.02	0.02	–
TLD 197	1200	2	Eu, Gd	1	–	0.00	0.02	2.10	0.70	0.07	95.96	–	–	–	–	0.02	0.01	–
TLD 198	1200	2	Eu, Gd	1	–	0.00	0.04	2.29	0.67	0.08	96.81	–	–	–	–	0.01	0.00	–
TLD 199	1200	2	Eu, Gd	1	–	0.00	0.02	2.68	0.65	0.02	96.15	–	–	–	–	0.00	0.00	–
TLD 200	1200	2	Eu, Gd	1	–	0.00	0.02	4.64	0.67	0.07	93.62	–	–	–	–	0.01	0.00	–
TLD 205	1200/800	2/9	Eu, Gd	1	–	0.00	0.00	4.50	0.38	0.04	90.09	–	–	–	–	0.02	0.00	–
TLD 206	1200/800	2/9	Eu, Gd	1	–	0.00	0.00	5.10	0.77	0.02	94.46	–	–	–	–	0.00	0.01	–
TLD 208	1200	2	Sm, Nd, Yb	1	–	0.00	0.02	2.80	0.45	0.02	96.83	–	–	0.00	0.00	–	–	0.01
TLD 209	1200	2	Sm, Nd, Yb	1	–	0.02	0.04	2.60	0.03	0.00	94.40	–	–	0.00	0.00	–	–	0.00
TLD 211	1200	2	La, Ce	1	–	0.00	0.00	1.59	0.27	0.01	97.62	0.01	0.01	–	–	–	–	–
TLD 212	1200	2	La, Ce	1	–	0.00	0.01	3.73	0.22	0.01	95.70	0.01	0.01	–	–	–	–	–
TLD 215	1200/800	2/9	Eu, Gd	1	–	0.01	0.02	0.04	0.05	0.10	99.01	–	–	–	–	0.02	0.00	–
TLD 216	1200/800	2/9	Eu, Gd	1	–	0.02	0.00	1.30	0.00	0.04	99.20	–	–	–	–	0.00	0.00	–
TLD 218	1200	2	Sm, Nd, Yb	1	–	0.10	0.08	15.70	0.04	0.20	86.50	–	–	0.05	0.03	–	–	0.05
TLD 219	1200	2	Sm, Nd, Yb	1	–	0.70	0.02	16.20	0.20	0.50	84.40	–	–	0.09	0.03	–	–	0.07
TLD 225	1200	2	Eu, Gd	1	Cr	0.02	0.04	3.90	0.03	0.11	93.40	–	–	–	–	0.04	0.02	–
TLD 228	1200	2	Eu, Gd	1	Mg	0.00	0.00	31.60	0.02	0.16	70.30	–	–	–	–	0.00	0.02	–
TLD 232	1200	2	Eu, Gd	1	V	0.12	0.06	3.80	0.19	0.36	95.24	–	–	–	–	0.04	0.02	–